Karlsruhe Institute of Technology

Finite Difference Modelling of Rayleigh Waves with Nonuniform Grid Spacing

-

Finite Differenzen Modellierung von Rayleigh Wellen mit variablen Gitterabständen

Bachelor's Thesis of

Marius Causemann

at the Department of Physics
Geophysical Institute

Reviewer:	Prof. Dr. Thomas Bohlen
Second reviewer:	PD Dr. Pradyumn Kumar Shukla
Advisor:	Dr. Yudi Pan

January 2018 – April 2018

Geophysikalisches Institut (GPI)
Fakultät für Physik
Hertzstrasse 16
Geb. 6.42
76187 Karlsruhe

I declare that I have developed and written the enclosed thesis completely by myself, and have not used sources or means without declaration in the text.

Karlsruhe, 16.04.2018

. . . .

(Marius Causemann)

Abstract

The finite difference method is a widely used technique for the computation of elastic wave propagation in heterogeneous media in presence of a free surface. However, finite-difference simulations require a high spatial resolution of the computational grid to avoid the introduction of numerical errors. The necessary resolution to achieve accurate results highly depends on the distribution of elastic parameters in the medium. The widely used rectangular grid with uniform spacing results in disproportional high spatial sampling in regions of high velocity, as the grid spacing has to be chosen with respect to the minimal wavelength occurring, which is linearly linked with the velocity of the propagating wave. This becomes especially important when considering the effect of a free surface due to the occurance of Rayleigh waves, that require a even higher spatial resolution. Surface topography even accentuates this problem, since it further tightens the resolution requirements.

In this thesis a finite difference method based on the application of a rectangular grid with nonuniform grid spacing is implemented. It introduces the possibility to adjust the resolution of the finite-difference computation to the requirements of the different areas of the model. Especially the high spatial resolution required for accurate simulation of Rayleigh waves suggests the use of a fine grid at the free surface and a coarser grid at the deeper part of the model. The effect of the application of a nonuniform grid with exponentially increasing grid spacing in the vertical direction on the accuracy and the computational cost of the method is investigated. Therefore, homogeneous and heterogeneous models of the subsurface are taken into consideration and the performance of both uniform and nonuniform grids is evaluated and compared. The results of this work reveal, that the approach of nonuniform grid spacing provides a significant increase of efficiency by simultaneously reducing the computational cost and increasing the accuracy. For heterogeneous models, the problem of alignment of model discontinuities and grid spacing arises and requires the adoption of the grid to the structure of the model.

Zusammenfassung

Um die Ausbreitung seismischer Wellen entlang einer freien Oberfläche mit heterogenem Untergrund zu simulieren, ist Nutzung der Finite-Differenzen-Methode weit verbreitet. Um große numerische Fehler des Verfahrens zu vermeiden, muss eine hohe Auflösung des Berechnungsgitters gewährleistet werden. Diese hängt stark von der Verteilung der elastischen Materialparameter des betrachteten Untergrundmodels ab. Die Verwendung einer versetzten Gitteranordnung mit gleichbleibenden Gitterabständen führt zu einem unnötig engmaschigen Gitter in Bereichen hoher Geschwindigkeit, da die Gitterweite abhängig von der minimalen auftretenden Wellenlänge gewählt werden muss, die proportional zu der Ausbreitungsgeschwindigkeit der seismischen Wellen ist. Dies wird im Falle der Modellierung einer freien Oberfläche weiter verschärft, da diese zum Auftreten von Oberflächenwellen führt, die eine sehr hohe räumliche Auflösung notwendig machen.

Im Rahmen dieser Arbeit wird eine Finite-Differenzen-Methode mit variablen Gitterabständen implementiert. Dies ermöglicht, die räumliche Auflösung des Verfahrens an die Anforderungen unterschiedlicher Regionen des Untergrundmodells anzupassen. Besonders durch die hohe Auflösungsanforderung der Simulation von Rayleigh Wellen liegt die Nutzung eines feinen Gitters nahe an der Oberfläche und eines gröberen Gitters in tieferen Regionen des Modells nahe. Der Effekt der Anwendung exponentiell ansteigender Gitterabstände in vertikaler Richtung auf die Genauigkeit und den Berechnungsaufwand des Verfahrens wird untersucht. Dazu werden homogene und heterogene Untergrundmodelle betrachtet und kostante und variable Gitter im Hinblick auf ihr Leistungsvermögen verglichen. Dadurch kann gezeigt werden, dass durch den Ansatz variabler Gitterabstände ein signifikanter Anstieg der Effizienz des Finite-Differenzen Verfahrens erreicht werden kann. Sowohl eine Senkung des Berechnungsaufwands als auch eine Erhöhung der Genauigkeit können gleichzeitig verwirklicht werden. Bei der Simulation heterogener Modelle tritt das Problem der korrekten Positionierung von Diskontinuitäten der Materialparameter auf, falls diese durch den erhöhten Gitterabstand nicht ausreichend präzise representiert werden können. Dadurch wird die Anpassung des Gitters an die Modelstruktur notwendig.

Contents

Abstract i

Zusammenfassung iii

1 Introduction 1
- 1.1 Background 1
  - 1.1.1 Relevance of Computation of Wave Propagation 1
  - 1.1.2 Comparison of Numerical Methods 1
- 1.2 Approach to a Solution 3
- 1.3 Research Questions 3

2 Seismic Wave Propagation 5
- 2.1 The Elastic Wave Equation 5
  - 2.1.1 Initial and Boundary Conditions 6
- 2.2 Types of Seismic Waves 8
  - 2.2.1 Body Waves 8
  - 2.2.2 The Rayleigh Wave 8

3 The Finite Difference Method 11
- 3.1 Example: Derivation of a Fourth Order Central Finite Difference Operator 11
- 3.2 Matrix Formulation of the Finite Difference Method 12
- 3.3 Discretization of the Elastic Wave Equation 15
  - 3.3.1 The Standard Staggered Grid 15
  - 3.3.2 Parameter Averaging 17
- 3.4 Nonuniform Finite Difference Operator 17
  - 3.4.1 Nonuniform Discretization Models 19
  - 3.4.2 Example: Exponentially Increasing Grid Spacing with Depth 20
- 3.5 Matrix Formulation of Differential Operators on Nonuniform Standard Staggered Grids 23
- 3.6 Implementation of the Free Surface Condition 24
  - 3.6.1 The Homogeneous Approach 25
  - 3.6.2 The Heterogeneous Approach 25
- 3.7 Implementation of Absorbing Boundary Conditions 26
- 3.8 Stability and Dispersion Criteria 27
  - 3.8.1 Stability Criterion 27
  - 3.8.2 Dispersion Criterion 28

4 Analysis of Numerical Results **29**
- 4.1 Characteristics of the Implemented Algorithm . . . 29
- 4.2 Benchmark of the NFD Implementation . . . 29
  - 4.2.1 Model Setup . . . 30
  - 4.2.2 Error vs. Spatial Resolution . . . 30
  - 4.2.3 Error vs. Offset . . . 31
  - 4.2.4 Comparison of Waveforms . . . 31
- 4.3 Comparison of Nonuniform and Uniform Grids . . . 34
  - 4.3.1 Measurement of the Computational Cost . . . 34
  - 4.3.2 Model 1: The Homogeneous Halfspace . . . 34
  - 4.3.3 Heterogeneous Models . . . 36
  - 4.3.4 Resampling of Material Parameter . . . 36
  - 4.3.5 Model 2: One Layer Overlaying Halfspace . . . 37
  - 4.3.6 Model 3: Gradient Increase Overlaying Homogeneous Halfspace 40
  - 4.3.7 Model 4: Low Velocity Layer . . . 43
  - 4.3.8 Model 5: Topography Overlaying Homogeneous Halfspace . . . 45
  - 4.3.9 Model 6: Vertical Fault with Low- and High-Velocity Bodies . . . 48

5 Conclusion **51**
- 5.1 Summary . . . 51
- 5.2 Outlook . . . 52

Bibliography **53**

List of Figures

2.1 Illustration of the Absorbing Boundary region Placement 7

3.1 Staggered Grid Scheme 15
3.2 Distances for Differential Operator 17
3.3 Nonuniform Standard Staggered Grid 18
3.4 Illustration of exponential increase of grid spacing 21
3.5 Effect of Exponential Increase of Grid Spacing on the Finite Difference Coefficients 22
3.6 Illustration of the Vacuum Formalism 26

4.1 Convergence of the Finite Difference Solution 32
4.2 Seismogram of the Benchmark Case 33
4.3 Benchmark of the homogeneous halfspace 35
4.4 Relative error in dependency of receiver offset of Model 2: One Layer Overlaying Homogeneous Halfspace 38
4.5 The vertical and horizontal velocity component of the receiver with maximum offset of Model 2: One Layer Overlaying Homogeneous Halfspace . 39
4.6 Relative error in dependency of the interface depth 40
4.7 Relative error in dependency of receiver offset of Model 3: Gradient Increase Overlaying Homogeneous Halfspace 41
4.8 The vertical and horizontal velocity component of the receiver with maximum offset of Model 3: Gradient Increase Overlaying Homogeneous Halfspace 42
4.9 Relative error in dependency of receiver offset of Model 4: Low Velocity Layer 43
4.10 The vertical and horizontal velocity component of the receiver with maximum offset of Model 4: Low Velocity Layer 44
4.11 Relative error in dependency of receiver offset of Model 5: Topography Overlaying Homogeneous Halfspace 46
4.12 Snapshot of the wavefield (v_z-component) of the nonuniform grid of Model 5: Topography Overlaying Homogeneous Halfspace 46
4.13 The vertical and horizontal velocity component of the receiver with maximumoffset of Model 5: Topography Overlaying Homogeneous Halfspace 47
4.14 Heterogeneous benchmark model with a vertical fault, a low and fast velocity anomaly 48
4.15 Comparison between the synthetic waveforms of the vertical fault model 49

1 Introduction

1.1 Background

1.1.1 Relevance of Computation of Wave Propagation

The capability to compute the propagation of elastic waves in heterogeneous media in the presence of a free surface is required by a variety of geophysical and geotechnical applications, such as earthquake studies, reservoir monitoring and geophysical near-surface exploration. Especially in the context of full waveform inversion (FWI), a technique that iteratively improves the model of the subsurface by comparison of computed and observed data, the efficient calculation of the propagating waves is crucial. This is due to the fact, that for each iteration of the FWI algorithm several completions of the forward computation are required. Apart from geophysical applications the simulation of elastic waves plays an important role in such diverse fields as ultrasonic imaging and non-destructive testing.

1.1.2 Comparison of Numerical Methods

The propagation of seismic waves can be modelled by a set of partial differential equations, that describe the relation of external forces, the displacement fields and the distribution of density and elastic parameters in the subsurface. Since analytical solutions to this problem do not exist for general heterogeneous media, various numerical approaches to solve the seismic wave equations were developed in the past decades. Each of these methods show specific advantages and disadvantages, that make careful weighting in respect of the intended field of application necessary (Fichtner 2010).

The Finite Difference Method The finite difference method can be considered as the first numerical method to be applied in the field of numerical computation of seismic wave propagation (Fichtner 2010) . First of all, space and time are discretized on a finite number of grid points, that are usually defined on an evenly spaced rectangular grid. Based on that, the fundamental idea of the finite difference method is the replacement of the derivatives by finite quotient equations, which involve the evaluation of the neighboring grid points. Great progress in the simulation of seismic waves with the finite difference technique was achieved by the introduction of the Standard Staggered Grid by Madariaga (1976) and Virieux (1986). Following this approach, different components of one physical parameter are defined at different staggered locations. This yields the main benefit of reducing the necessary spatial resolution of the computation grid to avoid the introduction of numerical errors such as numerical dispersion. The main advantages of the finite difference method are its relatively low computational cost and its high accuracy in the modelling of body wave propagation (Fichtner 2010).

The Finite Element Method The Finite Element method is based on the decomposition of the computational domain into disjoint subdomains. The field variables in each of those subdomains (called elements) are then approximated by polynomials of low order. The problem is thereby reduced to a linear system of the polynomial coefficients. Note that the continuity condition between the elements is explicitly fulfilled. On the one hand, this approach yields the main advantage of being easily applicable to irregular shaped geometries, that exemplarily occur at the free surface or internal discontinuities. On the other hand, the numerical dispersion resulting from the low order polynomial approximation is comparatively large (Fichtner 2010).

The Pseudospectral Method The fundamental idea of pseudospectral methods is the calculation of spatial derivatives in the Fourier Domain. At first, the seismic wave equation is sampled at a finite number of grid points. At the next stage, a Fourier Transformation is performed and the spatial derivatives are calculated by multiplication with ik in the Fourier Domain.Here, i denotes the imaginary unit and k is the wavenumber. The inverse Fast Fourier Transformation finally yields the desired derivatives in the space domain. Since only two grid points per wavelength are theoretically necessary for the spatial sampling according to the Nyquist theorem, pseudospectral methods are superior to finite difference methods regarding numerical dispersion. Unfortunately, the global nature of the approximation of derivative prohibits the usage of this method in case of highly heterogeneous media (Fichtner 2010).

The Spectral Element Method The spectral elements method aims at combining the main advantages of the finite element method and the pseudospectral method. This is achieved by dividing the computational domain into disjoint subdomains. Like in finite element methods, this preserves the adaptability to irregular geometries. Within each element higher order spectral approximation are used, such as Chebyshev polynomials or Lagrange polynomials (Fichtner 2010).

After considering the presented methods for the simulation of seismic wave propagation, the finite difference method is chosen due to its comparatively low computational cost. It allows the computation of accurate synthetic values of velocity and displacement of particles, even for heterogeneous models with high contrast of the elastic material parameters. The grid size, which directly influences the computational efficiency of the numerical simulation, is chosen with respect to the minimum wavelength of seismic waves propagating through the medium. In FD modelling of shallow seismic wavefields, which is dominated by surface waves, at least 15 grid points per minimum wavelength are needed to achieve good accuracy (Bohlen and Saenger 2006). Since Rayleigh-wave wavelengths usually increase with depth (Socco, Comina, and Khosro Anjom 2017), it implies that the grid size chosen might be disproportional for the deep part of the model.

1.2 Approach to a Solution

One approach to solve this problem and significantly reduce the computational effort is the application of a rectangular grid with nonuniform spacing (Pitarka 1999). It introduces the possibility to adjust the resolution of the finite difference computation to the requirements of the different areas of the model. Especially the high spatial resolution required for accurate simulation of Rayleigh waves suggests the use of a fine grid at the free surface and a coarser grid at the interior of the model.

1.3 Research Questions

The suggested improvement of the finte difference method on uniform grids gives rise to the following questions, that will serve as guidelines for this Bachelor Thesis:

1. Do finite difference simulations on nonuniform grids deliver reasonable results?
2. Can using nonuniform grids save computation time (and memory) while preserving a high level of accuracy?
3. Which (model dependent) discretization provides a good tradeoff between computation time and numerical error in context of Rayleigh wave modelling?

In Chapter 2 the basic concepts and the underlying equations of of seismic wave propagation and different types of elastic waves are introduced.

Chapter 3 provides a detailed explanation of the finite difference method. The concept of discrete differential operators is introduced and the coefficients for operators of different orders are derived. Additionally, the Standard Staggered Grid (SSG) discretization of the seismic wave equations is discussed and finally the method is generalized to rectangular grids with nonuniform grid spacing. Furthermore special attention is paid to the implementation of the free boundary condition at the interface of air and the subsurface.

Chapter 4 deals with the analysis of the numerical results of various test cases. First, the convergence of the implemented algorithm is verified by comparison of the simulated seismograms and analytical solutions for the case of a homogeneous halfspace. Additionally, the relationship between the error introduced by a nonuniform grid with increasing grid spacing with depth and computational saving is investigated. Subsequently, the propagation of waves is calculated for various subsurface models on nonuniform grids and compared to the result of simulation with a uniform grid. This analysis is performed to verify if the results achieved for the case of a homogeneous halfspace still hold for more complex subsurface models.

2 Seismic Wave Propagation

2.1 The Elastic Wave Equation

In this section the equations that govern the propagation of elastic waves in a general medium are briefly discussed following the explanations in Shearer (2009) and Bohlen, De Nil, et al. (2016). From a mathematical point of view, the propagation of seismic waves can be described by a set of coupled partial differential equations. First of all, the momentum equation as generalization of Newton's Law to continuous media shall be considered. With the density ρ, the components of the stress tensor τ_{ij}, the particle velocity v_i and an external force f_i the equation

$$\rho \frac{\partial v_i}{\partial t} = \frac{\partial \tau_{ij}}{\partial x_j} \tag{2.1}$$

describes the change of momentum caused by a stress field and an external force. Note that the Einstein summation convention is used. In case of an isotropic elastic medium the reaction to the stress and displacement is governed by the linear relationship of stress and strain:

$$\tau_{ij} = \lambda \delta_{ij} \epsilon_{kk} + 2\mu \epsilon_{ij} \tag{2.2}$$

Here δ_{ij} is the Kronecker symbol, ϵ_{ij} are the components of the strain tensor and λ and μ are the Lamé coefficients. Furthermore, displacement u and strain ϵ are directly related:

$$\epsilon_{ij} = \frac{1}{2} \left(\frac{\partial u_j}{\partial x_i} + \frac{\partial u_i}{\partial x_j} \right) \tag{2.3}$$

The combination of both equations leads to the stress-displacement formulation of the elastic wave equation:

$$\begin{aligned} \rho \frac{\partial^2 u_i}{\partial t^2} &= \frac{\partial \tau_{ij}}{\partial x_j} + f_i \\ \tau_{ij} &= \lambda \epsilon_{kk} \delta_{ij} + 2\mu \epsilon_{ij} \\ \epsilon_{ij} &= \frac{1}{2} \left(\frac{\partial u_j}{\partial x_i} + \frac{\partial u_i}{\partial x_j} \right) \end{aligned} \tag{2.4}$$

This system of second order partial differential equations can be transformed into a first order hyperbolic system called stress velocity formulation by taking the time derivative of the stress and strain relations of the stress-displacement formulation above.

For the two-dimensional case this finally leads to the following set of five partial differential equations (Virieux 1986):

$$\begin{aligned}
\frac{\partial v_x}{\partial t} &= b\left(\frac{\partial \tau_{xx}}{\partial x} + \frac{\partial \tau_{xz}}{\partial z}\right)\\
\frac{\partial v_z}{\partial t} &= b\left(\frac{\partial \tau_{xz}}{\partial x} + \frac{\partial \tau_{zz}}{\partial z}\right)\\
\frac{\partial \tau_{xx}}{\partial t} &= (\lambda + 2\mu)\frac{\partial v_x}{\partial x} + \lambda\frac{\partial v_z}{\partial z}\\
\frac{\partial \tau_{zz}}{\partial t} &= (\lambda + 2\mu)\frac{\partial v_z}{\partial z} + \lambda\frac{\partial v_x}{\partial x}\\
\frac{\partial \tau_{xz}}{\partial t} &= \mu\left(\frac{\partial v_x}{\partial z} + \frac{\partial v_z}{\partial x}\right)
\end{aligned} \tag{2.5}$$

2.1.1 Initial and Boundary Conditions

To compute the solution of the seismic wave equation, the initial and boundary conditions of the problem need to be defined.

Initial Conditions Prior to the start of the external force, the particle velocity v as well as the stress τ need to satisfy the initial condition of being equal to zero.

Dirichlet and Neumann Boundary Conditions The most common boundary conditions for differential equations are Dirichlet and Neumann Boundary conditions. While the former states, that the value of the considered function has to equal a defined value at the boundary of the computational domain, Neumann boundary conditions require the derivatives to attain a predefined value. Since both conditions cause artificial reflections at the boundaries, they do not play an important role in seismic modelling.

The Traction Free Boundary Condition Seismic modelling is often performed in the presence of an interface of air and the subsurface. Since the normal components of the stress tensor vanish at the interface, this is usually referred to as the free surface condition:

$$\tau \cdot \hat{n} = 0 \tag{2.6}$$

where $\hat{n}$ is the unit vector normal to the interface. It follows

$$\tau_{zz} = 0 \quad \tau_{xz} = 0 \tag{2.7}$$

at the free surface.

Absorbing Boundary Conditions The size of the computational grid is one of the main factors determining the computational cost of the simulation. Therefore, the domain should be chosen as small as possible. This makes the absorption of the seismic energy at

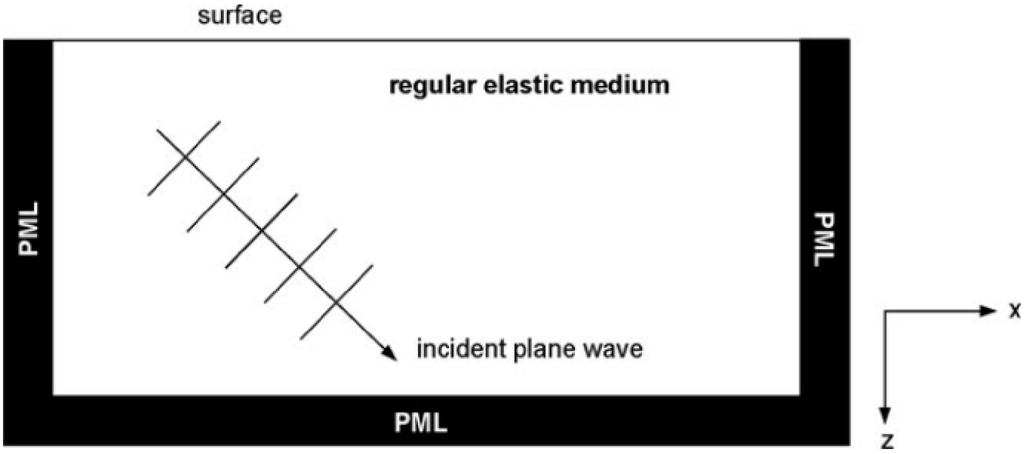

Figure 2.1: At the left, right and bottom boundaries of the computational domain absorbing boundary regions are placed. Within this the elastic wave equation is modified such that incident plane waves rapidly decay (Fichtner 2010)

the model boundaries necessary, as it would otherwise be reflected and cause spurious artifacts in the recorded data. This can be achieved by the application of so-called Perfectly-Matched-Layers (PML) at the boundary regions of the model, as illustrated in Figure 2.1. The following explanation is mainly based on the work of Komatitsch and Martin (2007), who modified the concept of the PML regions to so called Convolutional Perfectly Matched Layers. These have the benefit of higher effectiveness for waves with grazing incidence and do not require the splitting of the wavefield in parallel and perpendicular parts (in contrast to the classical PML formulation).

The main idea of the PML concept is the introduction of a new complex coordinate $\tilde{x}$

$$\tilde{x}(x) = x - \frac{i}{\omega} \int_0^x d_x(s) ds \tag{2.8}$$

that leads to exponentially decaying wave solutions in the PML region. The damping behavior is determined by the damping profile d_x, that is zero outside and some positive value inside the PML. The variable ω represents the angular frequency. This leads to a change of the spatial derivatives:

$$\partial_{\tilde{x}} = \frac{i\omega}{i\omega + d_x} \partial_x = \frac{1}{s_x} \partial_x \tag{2.9}$$

with s_x being defined by

$$s_x = \frac{i\omega + d_x}{i\omega}. \tag{2.10}$$

The C-PML concept generalizes this equation by introducing two real valued parameter $\alpha_x \geq 0$ and $\kappa_x \geq 1$. With these new variables s_x is redefined as

$$s_x(\omega) = \kappa_x \frac{d_x}{\alpha_x + i\omega}. \tag{2.11}$$

After going back to time domain and some calculus the spatial derivative $\partial_{\tilde{x}}$ is finally transformed in:

$$\partial_{\tilde{x}} = \frac{1}{\kappa_x}\partial_x + \zeta(t) * \partial_x \tag{2.12}$$

with

$$\zeta(t) = -\frac{d_x}{\kappa_x^2}\Theta(t)e^{-(d_x/\kappa_x+\alpha_x)t} \tag{2.13}$$

where $\Theta(t)$ is the Heavyside-Distribution. Thus, replacing the derivatives in the PML region by expression defined in Equation 2.12 yields the desired decay of wave amplitudes at the boundaries of the model.

2.2 Types of Seismic Waves

The first distinction for category formation of seismic waves is between surface and body waves. While body waves travel in the interior of the body, surface waves only occur at interfaces of the elastic medium.

2.2.1 Body Waves

Two different types of body waves exist, which are named after their arrival times: the primary P-wave and the secondary S-wave. While the P-waves are compressional waves where the particle displacement is in the same direction as the propagation of the wave, the S-waves are shear waves with particle motion perpendicular to the direction of energy transport.

The speed of both wave types depends on the elastic parameter of the medium:

$$v_p = \sqrt{\frac{\lambda + 2\mu}{\rho}} \quad \text{and} \quad v_s = \sqrt{\frac{\mu}{\rho}} \tag{2.14}$$

The relation of the velocity of both wave types can be expressed by the so-called Poisson's Ratio, which is defined as:

$$\nu = \frac{v_p^2 - 2v_s^2}{2(v_p^2 - v_s^2)} \tag{2.15}$$

It describes the ratio of transverse strain and longitudinal strain of the material and ranges from 0 to 0.5 (Berckhemer 1990).

2.2.2 The Rayleigh Wave

In presence of a free surface there also exits a Rayleigh wave solution of the seismic wave equation. It is guided along the free surface and the amplitude of the Rayleigh wave exponentially decays with depth. For this reason the energy spreads into a cylindrical region from the source and the geometrical damping declines with $1/r$ with the distance r from the source. Since body waves propagate radially, their damping is governed by $1/r^2$ and their amplitudes are significantly smaller, especially for greater distances. This makes the accurate modelling of Rayleigh waves a fundamental capability for applications such as earthquake studies and near-surface exploration.

The velocity of the Rayleigh wave is slightly less than the S-wave velocity depending on the Poisson's Ratio of the material. Exemplary the Rayleigh wave velocity v_R for a medium with a Poisson's Ratio of $\nu = 0.25$ is $v_R \approx 0.92 v_s$.

Another important feature for near-surface geophysical applications is the dispersion characteristic of Rayleigh waves. In case of a heterogeneous medium each frequency component of the wave travels at its characteristic velocity. This behavior allows the estimation of shear wave depth profiles by calculation and inversion of dispersion curves (Lorenzo 2014).

3 The Finite Difference Method

The finite difference method is a widely used technique for solving partial differential equations and plays an important role in modeling of seismic wave propagation. It is based on the idea of discretizing space and time on a computational grid. The partial derivatives of a function $u(x,t)$ at the position x^* on a grid with grid spacing h can then be calculated by evaluating $u(x,t)$ at the adjacent grid points and applying difference quotient equations. This approach leads to the definition of three differential operators:

$$D^+u(x^*) = \lim_{h\to 0}\frac{u(x^*+h)-u(x^*)}{h} \qquad \text{(Forward Operator)} \tag{3.1}$$

$$D^-u(x^*) = \lim_{h\to 0}\frac{u(x^*-h)-u(x^*)}{h} \qquad \text{(Backward Operator)} \tag{3.2}$$

$$D^cu(x^*) = \lim_{h\to 0}\frac{u(x^*+h)-u(x^*-h)}{2h} \qquad \text{(Central Operator)} \tag{3.3}$$

The accuracy of the finite difference method can be obtained by expanding a Taylor-Series expansion

$$u(x^*+h) = u(x^*) + hu'(x^*) + \frac{h^2}{2}u''(x^*) + \frac{h^3}{6}u'''(x^*) + \ldots + R(x^*) \tag{3.4}$$

with the remainder $R(x^*)$ and inserting the differential operator of interest for the approximated derivative. The lowest order of the step size h in the remainder term then defines the order of the finite difference operator.

Operators of higher order may be gained by considering more than only one neighboring grid point and determining coefficients, that make terms of lower order disappear. The central finite difference operator may then be denoted in the following form:

$$Du(x) = \sum_{m=-k}^{k} c_m \cdot u(x+m\cdot h) = [c_{-k} \quad c_{-k+1} \quad \ldots \quad c_{k-1} \quad c_k]u(x) \tag{3.5}$$

The term in square brackets is usually referred to as stencil.

3.1 Example: Derivation of a Fourth Order Central Finite Difference Operator

In the following the coefficients of a fourth order central finite difference operator will be derived exemplary (Leveugle n.d.).

Starting from the Taylor-Series expansion of a function $u(x)$:

$$u(x+kh) = u(x) + u'(x)kh + \frac{u''(x)}{2}(kh)^2 + \frac{u'''(x)}{6}(kh)^3 + \frac{u^{(4)}(x)}{24}(kh)^4 + O(h^5) \tag{3.6}$$

five equations for the grid point at position x and the two closest in both directions can be derived:

$$\begin{aligned}
u(x-2h) &= u(x) - 2hu'(x) + 2h^2u''(x) - \frac{4}{3}h^3u'''(x) + \frac{2}{3}h^4u^{(4)}(x) + O(h^5)\\
u(x-h) &= u(x) - hu'(x) + \frac{1}{2}h^2u''(x) - \frac{1}{6}h^3u'''(x) + \frac{1}{24}h^4u^{(4)}(x) + O(h^5)\\
u(x) &= u(x)\\
u(x+h) &= u(x) + hu'(x) + \frac{1}{2}h^2u''(x) + \frac{1}{6}h^3u'''(x) + \frac{1}{24}h^4u^{(4)}(x) + O(h^5)\\
u(x+2h) &= u(x) + 2hu'(x) + 2h^2u''(x) + \frac{4}{3}h^3u'''(x) + \frac{2}{3}h^4u^{(4)}(x) + O(h^5)
\end{aligned} \tag{3.7}$$

This system of equations can be transformed in matrix formulation:

$$\begin{bmatrix} u(x-2h)\\ u(x-h)\\ u(x)\\ u(x+h)\\ u(x+2h) \end{bmatrix} \approx \begin{bmatrix} 1 & -2h & 2h^2 & -\frac{4}{3}h^3 & \frac{2}{3}h^4\\ 1 & -h & \frac{1}{2}h^2 & -\frac{1}{6}h^3 & \frac{1}{24}h^4\\ 1 & 0 & 0 & 0 & 0\\ 1 & h & \frac{1}{2}h^2 & \frac{1}{6}h^3 & \frac{1}{24}h^4\\ 1 & 2h & 2h^2 & -\frac{4}{3}h^3 & \frac{2}{3}h^4 \end{bmatrix} \begin{bmatrix} u(x)\\ u'(x)\\ u''(x)\\ u'''(x)\\ u^{(4)}(x) \end{bmatrix} \tag{3.8}$$

Inverting the system directly yields the coefficients of the finite difference operators of up to the fourth order derivative:

$$\begin{bmatrix} 0 & 0 & 1 & 0 & 0\\ \frac{1}{12} & -\frac{2}{3} & 0 & \frac{2}{3} & -\frac{1}{12}\\ -\frac{1}{12} & -\frac{4}{3} & 0 & \frac{4}{3} & -\frac{1}{12}\\ -\frac{1}{2} & 1 & -\frac{5}{2} & -1 & \frac{1}{2}\\ 1 & -4 & 6 & -4 & 1 \end{bmatrix} \begin{bmatrix} u(x-2h)\\ u(x-h)\\ u(x)\\ u(x+h)\\ u(x+2h) \end{bmatrix} \approx \begin{bmatrix} u(x)\\ hu'(x)\\ h^2u''(x)\\ h^3u'''(x)\\ h^4u^{(4)}(x) \end{bmatrix} \tag{3.9}$$

The first derivative can consequently be calculated with fourth order accuracy with the following approximation:

$$u'(x) \approx \frac{u(x-2h) - 8u(x-h) + 8u(x+h) - u(x+2h)}{12h} \tag{3.10}$$

Higher derivatives and higher orders of accuracy may be obtained analogously.

3.2 Matrix Formulation of the Finite Difference Method

The finite difference method can be formulated as a matrix operation. For this purpose the discrete values of the function $u(x,z)$ on a grid sized $N_z \times N_x$ are defined as elements of the Matrix $U \in \mathbb{R}^{N_z \times N_x}$ in their natural order. To apply the discrete differential operator, an order has to be selected and the Matrix U has to be rearranged as a vector of the shape $\vec{u} \in \mathbb{R}^{N_z \cdot N_x}$. With lexicographical ordering this leads to:

$$U = \begin{bmatrix} u_{11} & u_{12} & \dots & u_{1N_x} \\ u_{21} & u_{22} & \dots & u_{2N_x} \\ \vdots & \vdots & \ddots & \vdots \\ u_{N_z 1} & u_{N_z 2} & \dots & u_{N_z N_x} \end{bmatrix} \Rightarrow \begin{bmatrix} u_{11} \\ u_{12} \\ \vdots \\ u_{1N_x} \\ u_{21} \\ u_{22} \\ \vdots \\ u_{2N_x} \\ \vdots \\ u_{N_z 1} \\ u_{N_z 2} \\ \vdots \\ u_{N_z N_x} \end{bmatrix} = \vec{u} \tag{3.11}$$

Assuming that the selected finite difference operator is of the form

$$Du(x) = \begin{bmatrix} c_{-2} & c_{-1} & c_0 & c_1 & c_2 \end{bmatrix} \quad u(x) \tag{3.12}$$

the operator can be written in matrix notation as a square block triagonal matrix $A \in \mathbb{R}^{(N_z \cdot N_x) \times (N_z \cdot N_x)}$:

$$A = \begin{bmatrix} T & 0 & \dots & 0 \\ 0 & T & \ddots & \vdots \\ \vdots & \ddots & \ddots & 0 \\ 0 & \dots & 0 & T \end{bmatrix} \tag{3.13}$$

with the matrix $T \in \mathbb{R}^{N_x \times N_x}$ representing the differential operator applied to one row of grid points:

$$T = \begin{bmatrix} c_0 & c_1 & c_2 & 0 & 0 & 0 & \dots & 0 \\ c_{-1} & c_0 & c_1 & c_2 & 0 & 0 & \dots & 0 \\ c_{-2} & c_{-1} & c_0 & c_1 & c_2 & 0 & \dots & 0 \\ 0 & c_{-2} & c_{-1} & c_0 & c_1 & c_2 & \dots & 0 \\ \vdots & \ddots & \ddots & \ddots & \ddots & \ddots & \ddots & \vdots \\ 0 & \dots & 0 & c_{-2} & c_{-1} & c_0 & c_1 & c_2 \\ 0 & \dots & 0 & 0 & c_{-2} & c_{-1} & c_0 & c_1 \\ 0 & \dots & 0 & 0 & 0 & c_{-2} & c_{-1} & c_0 \end{bmatrix} \tag{3.14}$$

Exemplary with the fourth order finite difference operator derived in chapter 3.1 the Matrix T becomes:

$$T = \frac{1}{12h} \begin{bmatrix} 0 & 8 & -1 & 0 & 0 & 0 & \dots & 0 \\ -8 & 0 & 8 & -1 & 0 & 0 & \dots & 0 \\ 1 & -8 & 0 & 8 & -1 & 0 & \dots & 0 \\ 0 & 1 & -8 & 0 & 8 & -1 & \dots & 0 \\ \vdots & \ddots & \ddots & \ddots & \ddots & \ddots & \ddots & \vdots \\ 0 & \dots & 0 & 1 & -8 & 0 & 8 & -1 \\ 0 & \dots & 0 & 0 & 1 & -8 & 0 & 8 \\ 0 & \dots & 0 & 0 & 0 & 1 & -8 & 0 \end{bmatrix} \tag{3.15}$$

Now multiplying the discrete operator with the vector $\vec{u}$ leads to the approximation:

$$Du(x) = A \cdot \vec{u} \tag{3.16}$$

Note that the derivative in another spatial direction can be calculated in at least two different ways. In the first place the differential operator can be discretized with respect the rearranged vector as described in Equation 3.2. This yields the disadvantage of making different matrices for the spatial directions necessary. Additionally, it implicates that the discrete operator in z-direction differs from the block diagonal form since the neighboring matrix elements are not adjacent in vector form. Alternatively, it is possible to leave the discrete operator unchanged and manipulate the matrix to vector mapping instead: if the transpose of the matrix U is ordered lexicographically, the derivative can be calculated in the same way for both spatial directions. For convenience, in the following this method is implicitly assumed.

This matrix formulation implicitly implements Dirichlet boundary conditions. This means that the values of all variables are zero outside the computational domain. Different boundary conditions can also be implemented in the matrix formulation, but do not play an important role in the considered case, since the model boundary is treated with special damping boundary regions (cf. Section 2.1.1).

The matrix formulation of the finite difference method yields significant benefits. First of all it is easy to implement, as no looping routine on all grid points is necessary. It also improves the readability of the code, as the equations can be written down in textbook like style. It also facilitates efficient and fast computation, since is introduces the possibility to exploit advantages of modern linear algebra packages (parallelization, efficiency, GPU computation).

At first glance the computational effort seems to be higher compared to an implementation based on looping routines, since it involves the storage and multiplication of large matrices. But this argument can be invalidated by considering the special structure of the discrete finite difference operator. The high memory consumption can be reduced to an negligible level by taking advantage of the repetitive structure of the matrix. The computational complexity of the matrix multiplication is cut to a level equivalent to the looping routine, if the sparsity of the matrix is exploited.

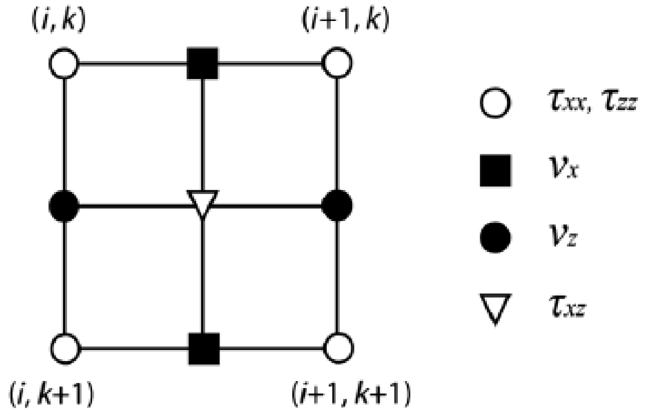

Figure 3.1: The standard staggered-grid scheme. The blank circles are the grid nodes, where the indices i and k describe the position in the grid. The stress components τ_{xx} and τ_{zz} as well as the Lamé coefficients λ and μ and the density ρ defined at the grid nodes, while the the velocity components v_x and v_z are represented by the black squares and the black circles respectively. The triangle placed at the midpoint of the cell is the stress component τ_{xz}. (Zeng et al. 2012)

3.3 Discretization of the Elastic Wave Equation

3.3.1 The Standard Staggered Grid

To model the propagation of seismic waves Madariaga (1976) and Virieux (1986) suggested the application of a standard staggered grid (SSG) as shown in Figure 3.1. Following this numerical scheme, different components of one physical parameter are defined at different staggered locations.

The usage of the SSG scheme yields the following benefits (Levander 1988):

- Stability for all values of Poisson's Ratio, any variation in material properties can be modeled correctly.
- Grid dispersion is small and relatively insensitive to Poisson's Ratio.
- Free surface boundary conditions are easily satisfied.

The proposed scheme is not only staggered in space, but also in time. The velocity components are computed at the time $(n + 0.5) \cdot \Delta t$ from the stress components at the time $n \cdot \Delta t$ and the stress components at $n \cdot \Delta t$ from the velocity components at $(n - 0.5) \cdot \Delta t$. This scheme is equivalent to the leapfrog time integration technique and yields second order accuracy in time (Bohlen, De Nil, et al. 2016).

Finally, the Standard Staggered Grid leads to the following discrete formulation of the seismic wave equation with the spatial indices i and k as defined in Figure 3.1 and the superscript n denoting the time step:

$$v^{n+1/2}_{z,[i,k+1/2]} = v^{n-1/2}_{z,[i,k+1/2]} + \Delt t \cdot b_{[i,k+1/2]} \left((D_z \tau^n_{zz})_{[i,k+1/2]} + (D_x \tau^n_{xz})_{[i,k+1/2]} \right)$$

$$v^{n+1/2}_{x,[i+1/2,k]} = v^{n-1/2}_{x,[i+1/2,k]} + \Delta t \cdot b_{[i+1/2,k]} \left((D_z \tau^n_{xz})_{[i+1/2,k]} + (D_x \tau^n_{xx})_{[i+1/2,k]} \right)$$

$$\tau^n_{xx,[i,k]} = \tau^{n-1}_{xx,[i,k]} + \Delta t \left[(\lambda_{[i,k]} + 2\mu_{[i,k]})(D_x v_x^{n-1/2})_{[i,k]} + \lambda_{[i,k]}(D_z v_z^{n-1/2})_{[i,k]} \right]$$

$$\tau^n_{zz,[i,k]} = \tau^{n-1}_{zz,[i,k]} + \Delta t \left[(\lambda_{[i,k]} + 2\mu_{[i,k]})(D_z v_z^{n-1/2})_{[i,k]} + \lambda_{[i,k]}(D_x v_x^{n-1/2})_{[i,k]} \right]$$

$$\tau^n_{xz,[i+1/2,k+1/2]} = \tau^{n-1}_{xz,[i+1/2,k+1/2]} + \Delta t \cdot \mu_{[i+1/2,k+1/2]} \left[(D_z v_x^{n-1/2})_{[i+1/2,k+1/2]} + (D_x v_z^{n-1/2})_{[i+1/2,k+1/2]} \right] \tag{3.17}$$

with the fourth order differential operators:

$$(D_z \tau^n_{zz})_{[i,k+1/2]} = c_1 \tau^n_{zz,[i,k-1]} + c_2 \tau^n_{zz,[i,k]} + c_3 \tau^n_{zz,[i,k+1]} + c_4 \tau^n_{zz,[i,k+2]}$$

$$(D_x \tau^n_{xx})_{[i+1/2,k]} = c_1 \tau^n_{xx,[i-1,k]} + c_2 \tau^n_{xx,[i,k]} + c_3 \tau^n_{xx,[i+1,k]} + c_4 \tau^n_{xx,[i+2,kk]}$$

$$(D_x \tau^n_{xz})_{[i,k+1/2]} = c_1 \tau^n_{xz,[i-3/2,k+1/2]} + c_2 \tau^n_{xz,[i-1/2,k+1/2]} + c_3 \tau^n_{xz,[i+1/2,k+1/2]} + c_4 \tau^n_{xz,[i+3/2,k+1/2]}$$

$$(D_z \tau^n_{xz})_{[i+1/2,k]} = c_1 \tau^n_{xz,[i+1/2,k-3/2]} + c_2 \tau^n_{xz,[i+1/2,k-1/2]} + c_3 \tau^n_{xz,[i+1/2,k+1/2]} + c_4 \tau^n_{xz,[i+1/2,k+3/2]}$$

$$(D_x v_x^{n-1/2})_{[i,k]} = c_1 v^{n-1/2}_{x,[i-3/2,k]} + c_2 v^{n-1/2}_{x,[i-1/2,k]} + c_3 v^{n-1/2}_{x,[i+1/2,k]} + c_4 v^{n-1/2}_{x,[i+3/2,k]}$$

$$(D_z v_z^{n-1/2})_{[i,k]} = c_1 v^{n-1/2}_{z,[i,k-3/2]} + c_2 v^{n-1/2}_{z,[i,k-1/2]} + c_3 v^{n-1/2}_{z,[i,k+1/2]} + c_4 v^{n-1/2}_{z,[i,k+3/2]}$$

$$(D_z v_x^{n-1/2})_{[i+1/2,k+1/2]} = c_1 v^{n-1/2}_{x,[i+1/2,k-1]} + c_2 v^{n-1/2}_{x,[i+1/2,k]} + c_3 v^{n-1/2}_{x,[i+1/2,k+1]} + c_4 v^{n-1/2}_{x,[i+1/2,k+2]}$$

$$(D_x v_z^{n-1/2})_{[i+1/2,k+1/2]} = c_1 v^{n-1/2}_{z,[i-1,k+1/2]} + c_2 v^{n-1/2}_{z,[i,k+1/2]} + c_3 v^{n-1/2}_{z,[i+1,k+1/2]} + c_4 v^{n-1/2}_{z,[i+2,k+1/2]} \tag{3.18}$$

Here, the variables c_i denote the finite difference coefficients and b is the buoyancy (inverse of density).

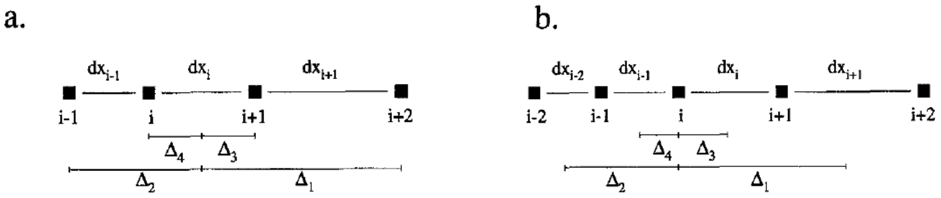

Figure 3.2: The distances Δ_i for derivatives calculated between grid points (a) and at grid point (b) (Pitarka 1999)

3.3.2 Parameter Averaging

As the physical parameters are defined at different staggered locations, the material parameters are required at the corresponding grid points. This can be achieved by local averaging, which is critical for the accuracy at strong discontinuities. Therefore, the density ρ and the shear modulus μ have to be arithmetically and harmonically averaged, respectively (Bohlen, De Nil, et al. 2016). As this averaging scheme is equivalent to the one used for the free surface condition, the equations can be found in Section 3.6.2.

3.4 Nonuniform Finite Difference Operator

In Pitarka (1999) a finite difference operator for rectangular Standard Staggered Grids with nonuniform grid spacing is presented. An example for such a nonuniform spacing can be found in Figure 3.3. In the following the derivation of this operator is briefly summarized.

The finite difference operator D_x can be expressed as

$$\begin{aligned} D_x u(x,z) &= c_1 u(x+\Delta_1, z) + c_2 u(x-\Delta_2, z) \\ &+ c_3 u(x+\Delta_3, z) + c_4 u(x-\Delta_4, z) \end{aligned} \tag{3.19}$$

with the distances Δ_i for derivatives calculated between grid points (a) and at grid point (b) as shown in Figure 3.2 (Pitarka 1999).

With the plane wave assumption

$$u(x,z) = u_z \exp(ikx) \tag{3.20}$$

differentiation leads to:

$$ik = c_1 \exp(ik\Delta_1) + c_2 \exp(-ik\Delta_2) + c_3 \exp(ik\Delta_1) + c_4 \exp(-ik\Delta_4) \tag{3.21}$$

Taylor Expansion up to order $O(\Delta_i^4)$ yields:

$$\exp(ik\Delta_i) \approx 1 + ik\Delta_i - \frac{1}{2}k^2\Delta_i^2 - \frac{1}{6}k^3\Delta_i^3 \tag{3.22}$$

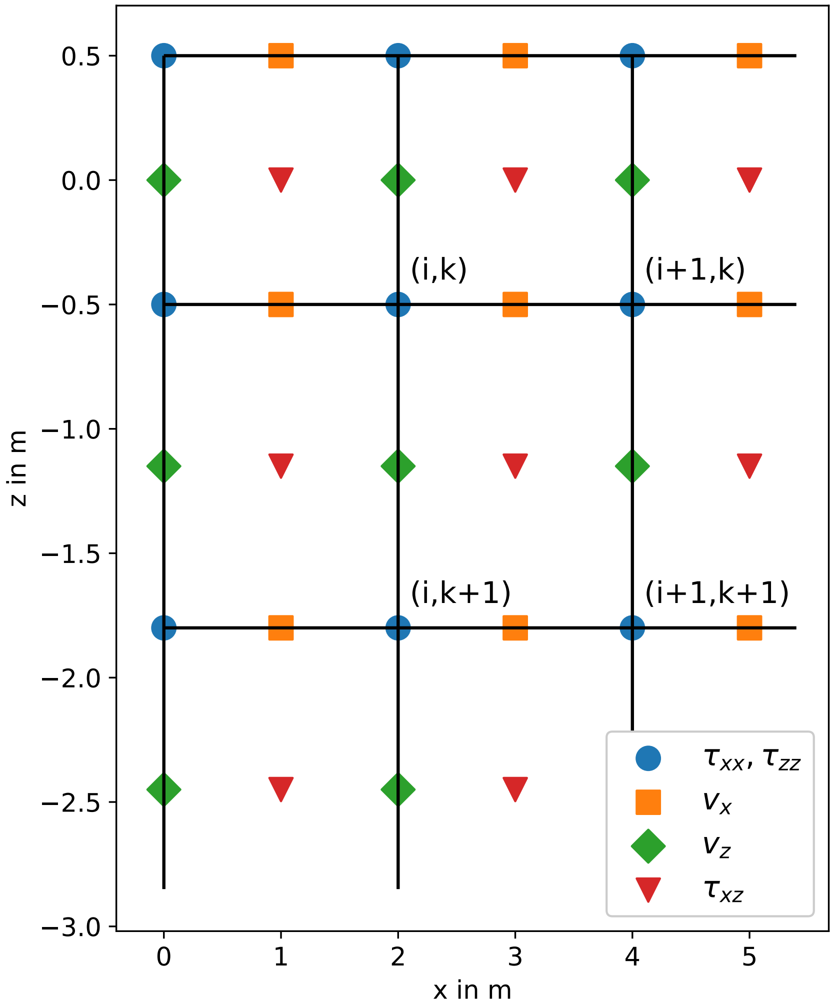
0.5
0.0
−0.5
−1.0
−1.5
−2.0
−2.5
−3.0
z in m
0
1
2
3
4
5
x in m
(i,k)
(i+1,k)
(i,k+1)
(i+1,k+1)
τ_{xx}, τ_{zz}
v_x
v_z
τ_{xz}

Figure 3.3: Example for a rectangular staggered finite difference grid with uniform grid spacing in x-direction and nonuniform grid spacing in z-direction

Then, equation 3.21 can be rearranged to:

$$\begin{aligned}
ik &= c_1 + c_2 + c_3 + c_4 \\
&\quad + ik(c_1\Delta_1 - c_2\Delta_2 + c_3\Delta_3 - c_4\Delta_4) \\
&\quad + \frac{ik^2}{2}(-c_1\Delta_1^2 - c_2\Delta_2^2 - c_3\Delta_3^2 - c_4\Delta_4^2) \\
&\quad + \frac{ik^3}{6}(-c_1\Delta_1^3 + c_2\Delta_2^3 - c_3\Delta_3^3 + c_4\Delta_4^3)
\end{aligned} \tag{3.23}$$

Solving the resulting linear system finally yields the finite difference coefficients c_i:

$$\begin{bmatrix} 1 & 1 & 1 & 1 \\ \Delta_1 & -\Delta_2 & \Delta_3 & -\Delta_4 \\ -\Delta_1^2 & -\Delta_2^2 & -\Delta_3^2 & -\Delta_4^2 \\ -\Delta_1^3 & \Delta_2^3 & -\Delta_3^3 & \Delta_4^3 \end{bmatrix} \begin{bmatrix} c_1 \\ c_2 \\ c_3 \\ c_4 \end{bmatrix} = \begin{bmatrix} 0 \\ 1 \\ 0 \\ 0 \end{bmatrix} \tag{3.24}$$

Considering the consumption of computational memory and time, note that two sets of coefficients (one set for derivatives calculated at the grid points and one between grid points) per dimension have to be calculated prior to the main simulation. Each set consists of 4 coefficients per grid point in the corresponding direction (N_x/N_z). This requires the solution of a 4×4 linear system for each grid point. Finally a total number of $8(N_x + N_z)$ coefficients have to be calculated and stored. This operation is is roughly linear to $\sqrt{N}$ and $\sqrt[3]{N}$ for the number of grid points N in the two dimensional and three dimensional cases respectively (assuming that $N_x \approx N_z(\approx N_y)$). Hence, the effort for the use of nonuniform finite difference operators can be considered relatively small compared to the the simulation itself and is therefore negligible. However, it is possible to further reduce the the computational cost by choosing a discretization model, that facilitates the computation of the finite difference coefficients (cf. Section 3.4.1).

3.4.1 Nonuniform Discretization Models

To take advantage of the possibility to define a nonuniform grid, it is necessary to identify reasonable discretization models. First of all, the requirements of an efficient discretization are:

- high resolution at the free surface to meet the requirements for accurate modelling of Rayleigh waves
- lower resolution in the deeper part of the model, that avoids spatial oversampling, but still ensures sufficient accuracy for the simulation of body waves
- reasonable increase of grid spacing with depth from the upper to the lower part of the model, that corresponds to the specific characteristics of Rayleigh waves

Since the amplitudes of Rayleigh waves exponentially decay with depth, an exponential increase of grid spacing is suggested. This leads to the following definition of the distance to the neighboring grid point in the vertical direction as function of the grid point index:

$$dz(\mathrm{k}) = \begin{cases} dx \cdot \beta & \text{, if k} \leq N_{above} \\ dx \cdot \beta \cdot (1+\alpha)^{k-N_{above}} & \text{, if k} > N_{above} \text{ and } dz(\mathrm{k}) \leq dz_{max} \\ dz_{max} & \text{, otherwise} \end{cases} \tag{3.25}$$

In the proposed nonuniform grid system, the grid size has a constant value of $dx \cdot \beta$ for the grids above the free surface, and then gradually increase with a constant factor of $(1+\alpha)$ until a maximum spacing of dz_{max} is reached. dz_{max} is chosen based on the required resolution for accurate modelling of body waves (at least 5 grid points per wavelength, Levander 1988). The parameter α aims at reducing the computational cost by decreasing the number of grid points, while β is supposed to improve the accuracy by increasing the resolution at the free surface. One advantage of using exponentially increasing grid system is that it leads to a constant change of the FD coefficients in the non-uniform grids. This feature greatly reduces the work in the calculation of FD coefficients from solving $2 \cdot N_z$ to only $2 \cdot n$ linear equations, where n is the order of the finite difference operator.

3.4.2 Example: Exponentially Increasing Grid Spacing with Depth

To illustrate the proposed discretization scheme, a one dimensional example is presented in this section. In Figure 3.4 the depth of each grid point is shown for a discretization with a minimal grid spacing $dx \cdot \beta = 0.1$ m at the free surface, a factor $\alpha = 0.2$, a maximal grid spacing $dz_{max} = 2$ and depth of 20 m. The resulting finite difference coefficients for the derivatives evaluated at the grid points are presented in Figure 3.5a. To clarify the reduced computational effort of the calculation of the coefficients, the quantity $c_i \cdot (1+\alpha)^k$ is plotted in Figure 3.5b. Since the values of the coefficients only change with the factor $1/(1+\alpha)$ from one grid point k to another, $c_i \cdot (1+\alpha)^k$ is constant in the part of the grid with exponentially increasing spacing. Therefore, the computational effort to calculate the derivative coefficients is limited to solving a constant number of linear systems.

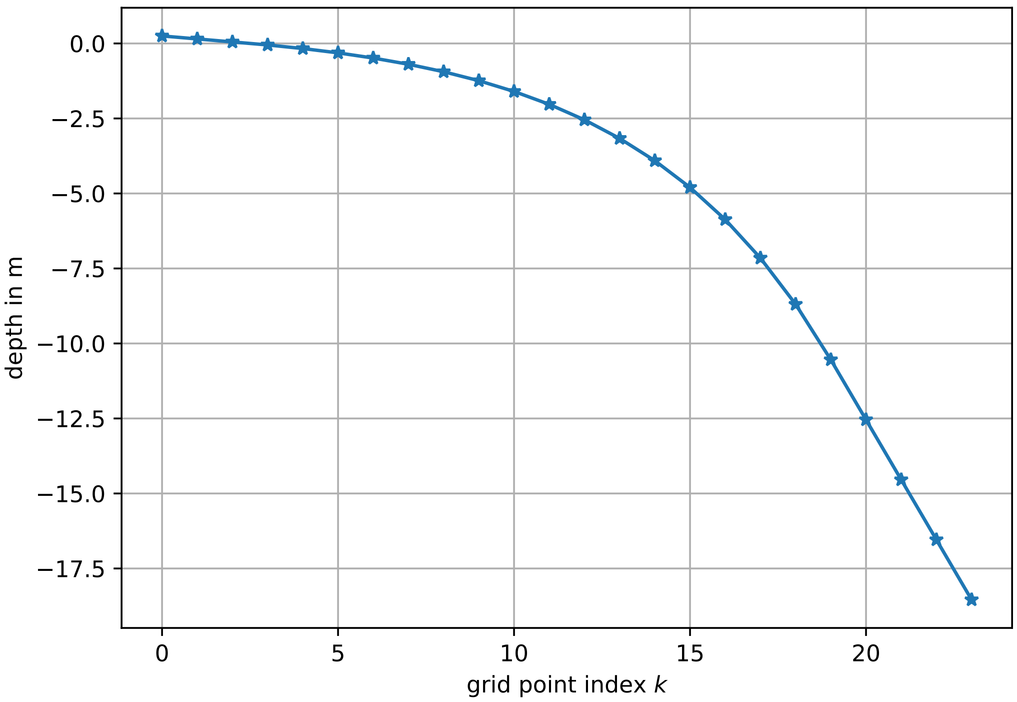

Figure 3.4: Illustration of exponential increase of grid spacing with depth for a discretization with a minimal grid spacing $dx \cdot \beta = 0.1\,\mathrm{m}$ at the free surface, a factor $\alpha = 0.2$ and a maximal grid spacing $dz_{max} = 2$.

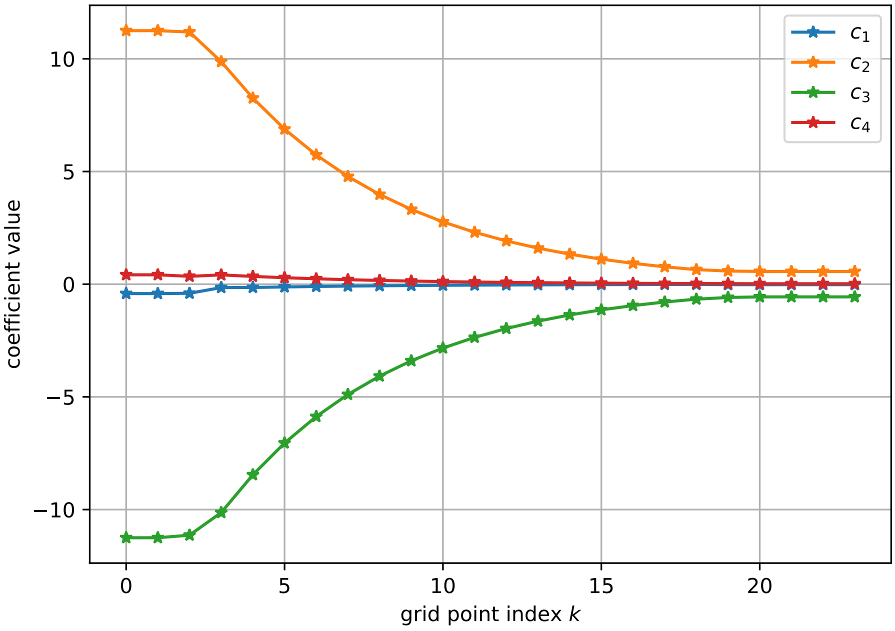

(a)

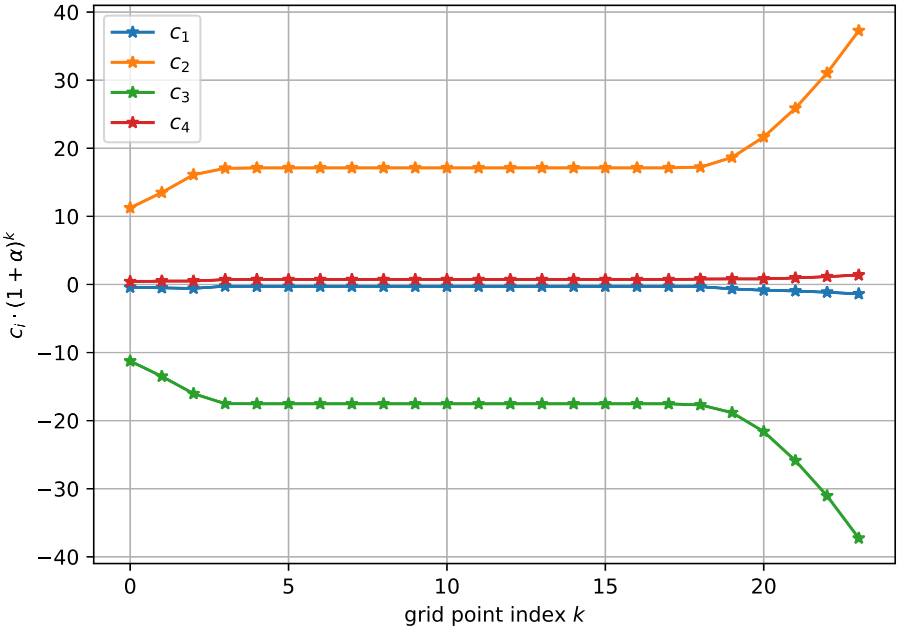

(b)

Figure 3.5: The values of the finite difference coefficients c_i for a nonuniform grid with exponentially increasing grid spacing with depth (a) and the quantity $c_i \cdot (1+\alpha)^k$ for a nonuniform grid with exponentially increasing grid spacing with depth (b)

3.5 Matrix Formulation of Differential Operators on Nonuniform Standard Staggered Grids

The implementation of the nonuniform finite difference operators on a Standard Staggered Grid requires special attention to the positioning of the coefficients in the matrix representing the discrete finite difference operator because the derivatives are calculated at different locations than the variable itself. Following the notation of Section 3.4 the stencil formulation is:

$$Du(x) = [c_1^k \quad c_2^k \quad c_3^k \quad c_4^k] \quad u(x) \tag{3.26}$$

Here the superscript $k \in \{0, \dots, N_x - 1\}$ indicates the index of the calculated derivative. Assuming that the number of variables located on the grid points is the same as the number of variables between the grid points in each dimension and the first variable between grid points is located between the first and second grid point, the following matrices T_{between} and $T_{\text{at Grid}}$ arise:

$$T_{\text{at Grid}} = \begin{bmatrix} c_3^0 & c_4^0 & 0 & 0 & 0 & 0 & \dots & 0 \\ c_2^1 & c_3^1 & c_4^1 & 0 & 0 & 0 & \dots & 0 \\ c_1^2 & c_2^2 & c_3^2 & c_4^2 & 0 & 0 & \dots & 0 \\ 0 & c_1^3 & c_2^3 & c_3^3 & c_4^3 & 0 & \dots & 0 \\ \vdots & \ddots & \ddots & \ddots & \ddots & \ddots & \ddots & \vdots \\ 0 & \dots & 0 & c_1^{N_x-3} & c_2^{N_x-3} & c_3^{N_x-3} & c_4^{N_x-3} & 0 \\ 0 & 0 & \dots & 0 & c_1^{N_x-2} & c_2^{N_x-2} & c_3^{N_x-2} & c_4^{N_x-2} \\ 0 & 0 & 0 & \dots & 0 & c_1^{N_x-1} & c_2^{N_x-1} & c_3^{N_x-1} \end{bmatrix} \tag{3.27}$$

$$T_{\text{between}} = \begin{bmatrix} \hat{c}_2^0 & \hat{c}_3^0 & \hat{c}_4^0 & 0 & 0 & 0 & \dots & 0 \\ \hat{c}_1^1 & \hat{c}_2^1 & \hat{c}_3^1 & \hat{c}_4^1 & 0 & 0 & \dots & 0 \\ 0 & \hat{c}_1^2 & \hat{c}_2^2 & \hat{c}_3^2 & \hat{c}_4^2 & 0 & \dots & 0 \\ \vdots & \ddots & \ddots & \ddots & \ddots & \ddots & \ddots & \vdots \\ 0 & \dots & 0 & \hat{c}_1^{N_x-4} & \hat{c}_2^{N_x-4} & \hat{c}_3^{N_x-4} & \hat{c}_4^{N_x-4} & 0 \\ 0 & 0 & \dots & 0 & \hat{c}_1^{N_x-3} & \hat{c}_2^{N_x-3} & \hat{c}_3^{N_x-3} & \hat{c}_4^{N_x-3} \\ 0 & 0 & 0 & \dots & 0 & \hat{c}_1^{N_x-2} & \hat{c}_2^{N_x-2} & \hat{c}_3^{N_x-2} \\ 0 & 0 & 0 & 0 & \dots & 0 & \hat{c}_1^{N_x-1} & \hat{c}_2^{N_x-1} \end{bmatrix} \tag{3.28}$$

The finite difference coefficients calculated as described in Section 3.4 are denoted by $\hat{c}$ for the variables between grid points and c for the variables at grid points. Finally, the discrete differential operator A can be formed by applying the appropriate matrix T as diagonal elements (cf. Section 3.2).

Exemplary, the discrete differential operator in matrix formulation of the grid presented in Section 3.4.1 can be found in Equation 3.29.

$$T_{\text{atGrid}} = \begin{bmatrix} -11.25 & 0.42 & 0.00 & 0.00 & 0.00 & 0.00 & 0.00 & 0.00 & 0.00 & 0.00 \\ 11.25 & -11.25 & 0.35 & 0.00 & 0.00 & 0.00 & 0.00 & 0.00 & 0.00 & 0.00 \\ -0.42 & 11.25 & -11.14 & 0.41 & 0.00 & 0.00 & 0.00 & 0.00 & 0.00 & 0.00 \\ 0.00 & -0.42 & 11.19 & -10.13 & 0.35 & 0.00 & 0.00 & 0.00 & 0.00 & 0.00 \\ 0.00 & 0.00 & -0.40 & 9.87 & -8.46 & 0.29 & 0.00 & 0.00 & 0.00 & 0.00 \\ \vdots & \ddots & \ddots & \ddots & \ddots & \ddots & \ddots & \ddots & \ddots & \vdots \\ 0.00 & 0.00 & 0.00 & -0.01 & 0.65 & -0.59 & 0.02 & 0.00 & 0.00 & 0.00 \\ 0.00 & 0.00 & 0.00 & 0.00 & -0.01 & 0.58 & -0.56 & 0.02 & 0.00 & 0.00 \\ 0.00 & 0.00 & 0.00 & 0.00 & 0.00 & -0.02 & 0.56 & -0.56 & 0.02 & 0.00 \\ 0.00 & 0.00 & 0.00 & 0.00 & 0.00 & 0.00 & -0.02 & 0.56 & -0.56 & 0.02 \\ 0.00 & 0.00 & 0.00 & 0.00 & 0.00 & 0.00 & 0.00 & -0.02 & 0.56 & -0.56 \end{bmatrix} \tag{3.29}$$

Finally, the discrete seismic wave equation on a nonuniform Standard Staggered Grid can be formulated in the following way:

$$\begin{aligned} v_z^{n+1/2} &= v_z^{n-1/2} + \Delta t \cdot b_z \left((\hat{A}_z \tau_{zz}^n) + (A_x \tau_{xz}^n) \right) \\ v_x^{n+1/2} &= v_x^{n-1/2} + \Delta t \cdot b_x \left((A_z \tau_{xz}^n) + (\hat{A}_x \tau_{xx}^n \right) \\ \tau_{xx}^n &= \tau_{xx}^{n-1} + \Delta t \left[(\lambda + 2\mu)(A_x v_x^{n-1/2}) + \lambda (A_z v_z^{n-1/2}) \right] \\ \tau_{zz}^n &= \tau_{zz}^{n-1} + \Delta t \left[(\lambda_{+} 2\mu)((A_z v_z^{n-1/2}) + \lambda((A_x v_x^{n-1/2}) \right] \\ \tau_{xz}^n &= \tau_{xz}^{n-1} + \Delta t \cdot \mu_{xz} \left[(\hat{A}_z v_x^{n-1/2}) + (\hat{A}_x v_z^{n-1/2}) \right] \end{aligned} \tag{3.30}$$

Here, the matrices $\hat{A}_i$ and A_i denote the discrete differential operator formed by the corresponding T matrices between and at the grid node, respectively.

3.6 Implementation of the Free Surface Condition

One key element for the accurate simulation of Rayleigh waves is the implementation of the interface between the elastic medium and air in the finite difference scheme. Because of the vanishing stress components in directions normal to the interface, this boundary is referred to as stress free surface condition (Bohlen, De Nil, et al. 2016). The existing approaches to this problem can be roughly divided into two aproaches: The Heterogeneous and the Homogeneous Approach.

3.6.1 The Homogeneous Approach

In the Homogeneous Approach the free surface condition is explicitly fulfilled by applying a special calculation scheme for the grid points directly at the interface. One widely used method for this is the image method. Following this method, the stress component τ_{zz} is explicitly set to zero at the free surface and τ_{xz} is imaged as odd function across the free surface (Bohlen and Saenger 2006). The main advantage of this method is that it delivers accurate results even for relatively coarse grids (Bohlen and Saenger 2006). The main drawbacks of the Homogeneous Approach are that it requires the application of different calculation schemes for different regions of the model and can only be easily applied to planar free surfaces.

3.6.2 The Heterogeneous Approach

The Heterogeneous Approach aims at overcoming the limitations of the Homogeneous approach by assuming that the boundary conditions are implicitly satisfied by the distribution of the elastic parameters in the model (Bohlen and Saenger 2006). This yields the advantages, that no explicit boundary condition needs to be implemented and surface topography can easily included in the model by setting the corresponding elastic parameter to zero. For this reason this method is also called Vacuum-Formalism. The use of the SSG makes local averaging of the material parameter necessary. Special attention should be paid to the averaging scheme, as it plays a critical role for the stability and accuracy of the simulation (Mittet 2002). Zeng et al. (2012) proposed an Improved Vacuum Formulation for the modeling of Rayleigh waves and internal discontinuities. They suggest volume harmonic averaging for the shear modulus μ and arithmetic averaging for the density, as performed by the following expressions:

$$\bar{b}_x = \begin{cases} 0 & \text{if } \rho_{i,k} = 0 \text{ and } \rho_{i+1,k} = 0 \\ \frac{2}{\rho_{i,k}+\rho_{i+1,k}} & \text{otherwise} \end{cases} \tag{3.31}$$

$$\bar{b}_z = \begin{cases} 0 & \text{if } \rho_{i,k} = 0 \text{ and } \rho_{i,k+1} = 0 \\ \frac{2}{\rho_{i,k}+\rho_{i,k+1}} & \text{otherwise} \end{cases} \tag{3.32}$$

$$\bar{\mu}_{xz} = \begin{cases} \left[\frac{1}{4}\left(\frac{1}{\mu_{i,k}} + \frac{1}{\mu_{i+1,k}} + \frac{1}{\mu_{i,k+1}} + \frac{1}{\mu_{i+1,k+1}}\right)\right]^{-1} & \text{if } \mu_{i,k}\mu_{i+1,k}\mu_{i,k+1}\mu_{i+1,k+1} \neq 0 \\ 0 & \text{otherwise} \end{cases} \tag{3.33}$$

This method is as well applicable to planar free surface cases as topography cases, as shown in figure Figure 3.6.

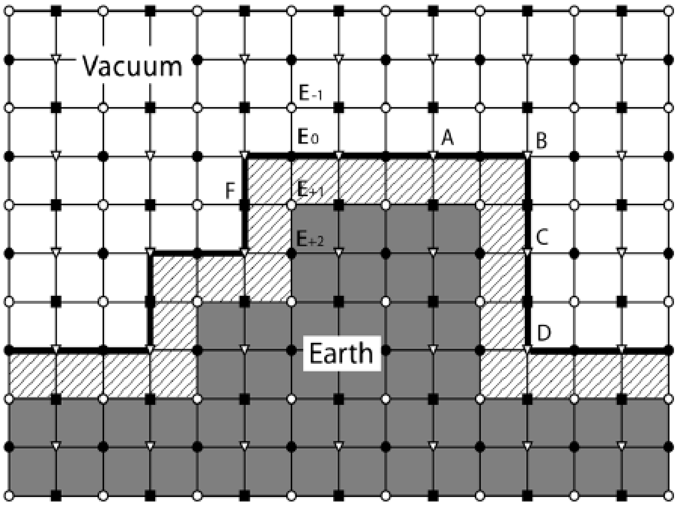

Figure 3.6: Grid distribution of the improved vacuum formulation in presence of surface topography. The shadowed area is a fictitious layer whose thickness is only half a cell size. The free surface in actual computation is represented by the bold solid line. All parameters above the free surface are set to zero during modelling. The oblique surface segment can be approximated by the staircase shape (Zeng et al. 2012)

3.7 Implementation of Absorbing Boundary Conditions

Following the presentation of the convolutional PML technique in Section 2.1.1 based on Komatitsch and Martin (2007) the implementation within the finite difference method is discussed in this section. Recall the fundamental idea of replacing the spatial derivatives:

$$\partial_{\tilde{x}} = \frac{1}{\kappa_x}\partial_x + \zeta(t) * \partial_x \tag{3.34}$$

with

$$\zeta(t) = -\frac{d_x}{\kappa_x^2}\Theta(t)e^{-(d_x/\kappa_x+\alpha_x)t} \tag{3.35}$$

This implies, that in the PML - regions the spatial derivatives have to be replaced by the sum of two terms: The original derivative (divided by a constant factor) and the convolution of the derivative with a given function $\zeta(t)$. This convolutional term ca be efficiently computed in context of the discrete staggered time scheme by a recursive convolution technique. For that reason a new memory variable Ψ_x^n is introduced and updated at each time step n by:

$$\Psi_x^n = b_x\Psi_x^{n-1} + a_x(\partial_x)^{n+1/2} \tag{3.36}$$

with

$$b_x = e^{-(d_x/\kappa_x+\alpha_x)\Delta t} \quad \text{and} \quad a_x = \frac{d_x}{\kappa_x(d_x+\kappa_x\alpha_x)}(b_x-1). \tag{3.37}$$

Finally the spatial derivative ∂_x is replaced by:

$$\partial_{\tilde{x}} = \frac{1}{\kappa_x}\partial_x + \Psi_x \tag{3.38}$$

From the numerical point of view it is interesting to note that the additional memory usage of this method is limited to eight additional arrays (one for each derivative) in the PML-region.

Ultimately the free parameters of the method have to be chosen. Collino and Tsogka (2001) suggested a damping profile d_x of the form:

$$d_x(x) = d_0 \left(\frac{x}{L}\right)^N \tag{3.39}$$

with the thickness of the damping region L and a factor d_0:

$$d_0 = -(N+1)v_p \frac{log(R)}{2L} \tag{3.40}$$

Furthermore, the following parameter have to be chosen with respect to the required damping behavior and structure of the model:

- the mean p-wave velocity v_p in the PML- region
- the exponent N of the damping profile
- the variable κ_x
- the variable α_x
- the reflection coefficient R. It is usually assumed to be $R \approx 10^{-4}$ (Bohlen, De Nil, et al. 2016).
- the number of grid points in the PML-region,

3.8 Stability and Dispersion Criteria

To achieve stable and accurate simulation results, certain dispersion and stability criteria have to be met.

3.8.1 Stability Criterion

As the applied time integration scheme is explicit, the maximal time step is limited and depends on the spatial grid spacing. According to Virieux (1986) the time step Δt, the grid spacing in vertical direction Δz and in horizontal direction Δx with the P-wave velocity v_p have to satisfy the following inequality:

$$v_p \Delta t \cdot \sqrt{\frac{1}{\Delta x^2} + \frac{1}{\Delta z^2}} < 1 \tag{3.41}$$

Greater time steps lead to unstable simulation results. This stability criterion is usually referred to as Courant-Friedrichs-Lewy stability condition. According to Pitarka (1999), an analytical derivation of the stability condition of the nonuniform grid is difficult to obtain, but is expected to be locally similiar to the stability condition of the uniform grid.

3.8.2 Dispersion Criterion

Besides the temporal resolution, the spatial resolution has to be chosen carefully. If the grid spacing $\Delta x/\Delta z$ is too coarse, numerical artifacts arise in the calculated solutions. As the resulting wavefields seem to show a behavior resembling the dispersion of the waves, this phenomenon is called grid dispersion or numerical dispersion (Bohlen, De Nil, et al. 2016). The criterion to predict the occurrence of numerical dispersion is the number of grid points per minimal wavelength λ_{min}(short: ppw). This can be calculated by:

$$ppw = \frac{\lambda_{min}}{\Delta x} = \frac{v_{min}}{f_{max}\Delta x} \tag{3.42}$$

Evidently, this quantity is dependent of the source characteristics, especially the maximal excited frequency f_{max}, and the minimal velocity v_{min} of the medium. Furthermore, the required ppw number depends on the order of the finite difference operator used and the expected accuracy of the simulation. According to Virieux (1986), Levander (1988) and Bohlen, De Nil, et al. (2016) it roughly varies from 5 to 10 for the simulation of body waves with an fourth order operator. The simulation of Rayleigh waves requires higher spatial resolution. Fichtner (2010) suggests a minimal ppw-number of 20 and Bohlen and Saenger (2006) reports that 15 to 30 grid points per wavelength are sufficient for accurate results.

4 Analysis of Numerical Results

In this chapter numerical results obtained by a newly implemented nonuniform finite difference software (short: NFD) will be discussed. At first, the main characteristics of the NFD are presented. Then its correctness is validated by examination of the convergence of the algorithm to an analytically obtained solution. At the next stage, the effect of the nonuniform grid spacing on the accuracy of the simulation result is examined and related with the computational saving provided by this method. Therefore, various subsurface models are simulated with different discretization and the results are compared with simulations with uniform grid spacing. This approach is expected to give answer to the research questions formulated in Section 1.3.

4.1 Characteristics of the Implemented Algorithm

Based on the theoretical considerations presented in the previous chapter, a finite difference algorithm with nonuniform grid spacing was implemented in the programming language Python 3. It features the following characteristics:

- object oriented implementation in Python 3
- matrix formulation of the finite difference method
- automatically generated nonuniform finite difference operator of fourth order
- second order time integration
- Standard Staggered Grid discretization of the two dimensional stress-velocity formulation of seismic wave propagation (Virieux 1986)
- Convolutional-PML boundary regions (Komatitsch and Martin 2007)
- implicit free surface condition implemented by the Improved Vacuum Formulation (Zeng et al. 2012)

4.2 Benchmark of the NFD Implementation

Initially the correctness of the implementation will be examined by comparison of the results of the NFD using a uniform grid with analytically computed seismograms. To achieve this goal the analytical solutions in case of an homogeneous halfspace are calculated by the Cagniard-De Hoop Technique (Berg et al. 1994). Since the numerical solution naturally shows small variations, the seismograms are also computed with the finite difference software SOFI2D to align the scale of errors. SOFI2D is a well established finite difference software developed at the chair of Applied Geophysics at the Geophysical Institute at KIT (Bohlen, De Nil, et al. 2016).

To quantify the differences between the analytical and finite difference seismograms the L_2-Norm is used (Bohlen and Saenger 2006):

$$L_2 = \frac{\sum_{l=0}^{N} (f(l\Delta t) - q(l\Delta t))^2}{\sum_{l=0}^{N} q(l\Delta t))^2} \tag{4.1}$$

Here $q(t)$ and $f(t)$ are the analytical and numerical solutions respectively and N is the number of time steps. Since this measure is rather sensitive to time shifts than the correctness of the wave form (Bohlen and Saenger 2006), plots of the seismograms are also shown for visual comparison.

4.2.1 Model Setup

For this numerical analysis a near-surface homogeneous halfspace model with the following specifications is used:

- model size: 60 m x 20 m
- time step: $\Delta t = 100\,\mu$s
- total simulation time $T = 0.4$ s

The Material parameters are specified in Table 4.2 and the source is modeled by a vertical point source excited by a Ricker wavelet :

$$s(t) = (1 - 2\tau^2)e^{-\tau^2} \quad \text{with} \quad \tau = \pi \left(t - \frac{1.5}{f} - t_0 \right) \cdot f \tag{4.2}$$

Here t is the time since start of the simulation, f is the peak frequency and t_0 is the source delay. The maximum frequency is assumed to be about twice as high as the peak frequency. The chosen parameterization can be found in Table 4.1. The receivers are equidistantly placed as detailed in Table 4.3.

4.2.2 Error vs. Spatial Resolution

To investigate the convergence of the finite difference method towards the analytical solution with increasing resolution, the presented model is calculated with various grid

Table 4.1: Source Parameterization for the Ricker Wavelet of the Convergence Test

source frequency	source depth	source x-position	source delay
30 Hz	1 m	5 m	0 s

Table 4.2: Material Parameter for the Convergence Test

	depth	S wave velocity v_s	P wave velocity v_p	density ρ
1. layer	0 m	220 m/s	500 m/s	2100 kg/m^3

Table 4.3: Receiver Placing for the Convergence Test

number of receivers	first receiver position	receiver distance	receiver depth
24	6 m	2 m	0 m

spacings. In Figure 4.1a the resulting L_2 Error (Equation 4.1) is shown for the NFD and SOFI2D solutions. It reveals, that both the SOFI2D and the NFD solution show very small deviations for high resolution simulations, which suggests that they converge towards the analytical solution in the considered test case. Still the SOFI2D code performs slightly better for all *ppw*-numbers, which is due to a different a implementation of the free surface condition. SOFI2D features an explicit boundary condition (image method) (Bohlen, De Nil, et al. 2016), that is reported to deliver more accurate results than Heterogeneous Approaches (Bohlen and Saenger 2006).

4.2.3 Error vs. Offset

The error of the finite difference simulation is usually dependent on the offset of the receiver, since it accumulates with greater distance from the source. Therefore, the misfit is calculated for different offsets for all spatial resolutions. The results are shown in Figure 4.1b. First of all, the SOFI2D results exhibit comparatively high error in the first traces. Apparently, the Vacuum Formulation is better suited for the modelling of near fields effects. Apart from that, the relative error rises with offset for the simulations with rather coarse grids, which may be explained by the accumulation of error with offset.

4.2.4 Comparison of Waveforms

To illustrate the accuracy achieved by the simulations with different grid spacings the horizontal and vertical velocity components of the receiver with greatest offset are shown in Figure 4.2. It reveals, that even for the lowest *ppw*-number of 14 an acceptable accuracy is achieved.

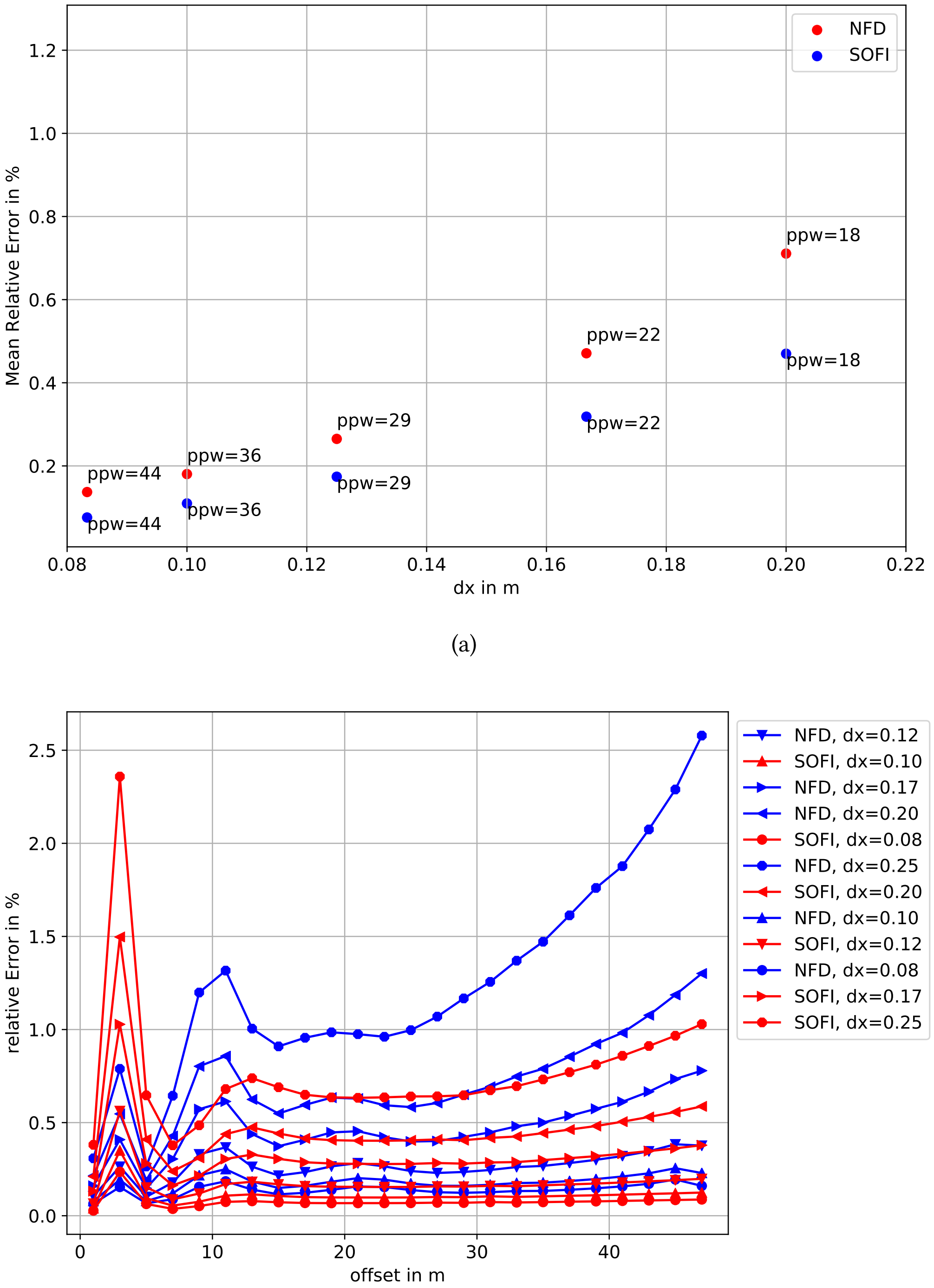

(a)

(b)

Figure 4.1: The L_2 Error in dependency of the grid spacing $dx = dz$ (b) and the L_2 Error in dependency of the offset (b)

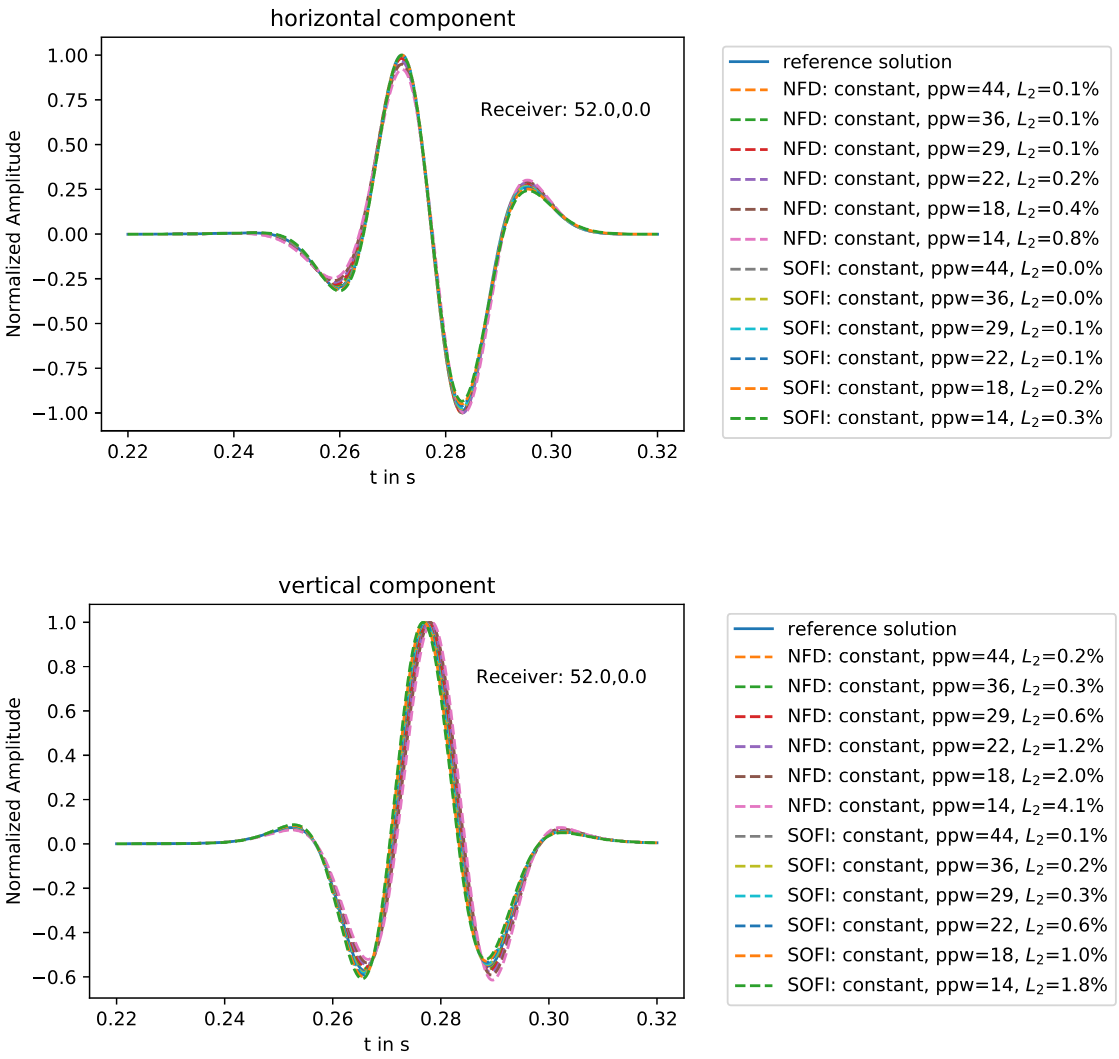

Figure 4.2: The vertical and horizontal velocity component of the receiver with maximum offset of the Benchmark Case

4.3 Comparison of Nonuniform and Uniform Grids

In this Section the results of uniform and nonuniform grids are compared regarding accuracy and computational cost. Therefore, first a method for measuring the computational effort related to the chosen grid is presented. Based on that, the results for various subsurface models are discussed.

4.3.1 Measurement of the Computational Cost

For the evaluation of different discretization of the subsurface, it is essential to measure the computational cost of the simulation. Since it is desirable to find a measure independent of the used hardware and the implementation details of the algorithm, the run time and memory consumption can not serve as basis for the evaluation. Instead, the number of grid points and the number of time steps are taken into consideration, because the computational cost is expected to be roughly linear in both quantities. Note that the time step length is not independent of the grid spacing. The Courant-Friedrichs-Lewy stability condition (cf. Section 3.8.1) constrains the maximum time step, which is crucial for the computational cost of the simulation. According to Fichtner (2010), the numerical error is dominated by the inaccuracies of the spatial discretization, as empirical studies have shown. Therefore, the time step is adopted to the spatial grid by setting it to 80% of the maximum value according to that criterion. Finally, the computational cost is measured by the product of number of grid points and necessary time steps.

4.3.2 Model 1: The Homogeneous Halfspace

Again, the simple case of a homogeneous halfspace with a model size of 60 m x 20 m and a total simulation time of $T = 0.3$ s is considered. The left, right and bottom boundary regions are implemented with a C-PML layer of 10 grid points. Further details can be found in Tables 4.4, 4.5 and 4.6 on the source parameterization, material parameter and the receiver placement, respectively.

The horizontal resolution is kept constant with a grid spacing of 0.2 m. The maximum vertical resolution is set to $dz_{max} = 0.8$ m. Wavefields are simulated with different α and β values, respectively. The simulation is also performed by using a uniform reference grid with a grid spacing of $dx = dz = 0.2$ m (corresponding to 18 grid points per minimum wavelength).

The synthetic result (Figure 4.3) shows that higher accuracy and lower computational effort can be achieved simultaneously when utilizing a nonuniform grid compared to the uniform grid. For the case in which $\beta = 1$, the saving of computational resources reaches 60 %, but the accuracy decreases rapidly with increasing grid size factor α. Considering

Table 4.4: Source Parameterization for the First Model: Homogeneous Halfspace

source frequency	source depth	source x-position
30 Hz	0 m	6 m

Table 4.5: Material Parameter for the First Model: Homogeneous Halfspace

	depth	S wave velocity v_s	P wave velocity v_p	density ρ
1. layer	0 m	220 m/s	500 m/s	2100 kg/m^3

Table 4.6: Receiver Placing for the First Model: Homogeneous Halfspace

number of receivers	first receiver position	receiver distance	receiver depth
24	10 m	2 m	0 m

the case where $\beta = 0.5$, we gain a relatively high accuracy in the simulated waveforms, at the expense of relatively low computational saving compared to the reference grid. Compared to a uniform grid with comparable accuracy, the gain of efficiency is particularly high. For example, with $\alpha = 0.1$ the relative error is on the same level as the error of a uniform grid with more than 3 times the cost of the reference grid, while the nonuniform grid simulation consumes less than 75 % of computational cost compared to the reference grid. Since both low computational cost and high accuracy in the simulated waveforms are desired simultaneously, $\beta = 2/3$ and $\alpha = 0.1$ are identified as a reasonable choice of parameterization. It provides the best trade-off between accuracy and computational efficiency among the choices in the nonuniform grid system.

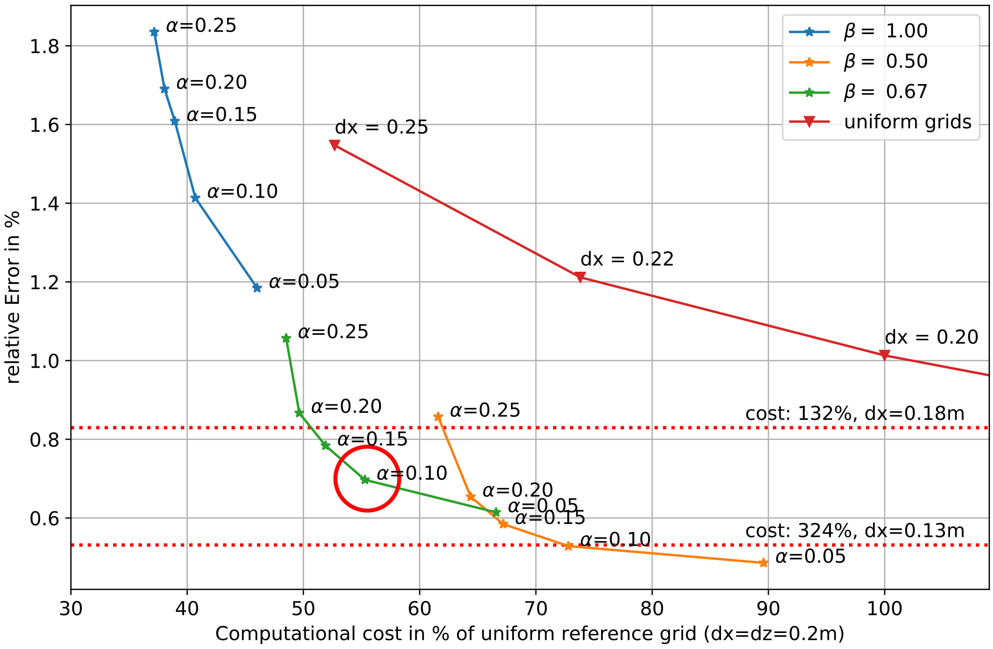

Figure 4.3: The computational effort as product of the number of time steps and grid points in percentage of a uniform reference grid (dx=0.2 m, $ppw = 18$) and the accuracy for various discretization. The dotted red lines denote the level of accuracy accomplished by uniform grids with different grid spacings.

Table 4.7: Source Parameterization for the Heterogeneous Models

source frequency	source depth	source x-position
30 Hz	0 m	5 m

Table 4.8: Receiver Placing for the Heterogeneous Models

number of receivers	first receiver position	reveiver distance	receiver depth
24	8 m	2 m	0 m

4.3.3 Heterogeneous Models

As a next step, different heterogeneous models with increasing complexity are considered. Since an analytical solution for this case is not available, the results of the NFD software with uniform and nonuniform grids are compared to pseudoanalytical solutions, which are calculated by using a high resolution uniform grid. Thereby, the effect of the differently spaced grids can be quantified.

The general setup except for the material parameter of all models is kept constant. The computational domain has a total size of 60 m x 2 m and a total simulation time of $T = 0.5$ s. C-PML boundary layers are applied at all sides except for the free surface. The source is excited by a vertical point source modelled with a Ricker Wavelet. The parameterization can be found in Table 4.7. The receiver are equidistantly placed at the free surface with a spacing described in Table 4.8.

Regarding the spatial discretization, a uniform grid with a spacing of $dx = dz = 0.1$ m is used for the computation of the pseudoanalytical solution. For comparison of the uniform and nonuniform grids, the horizontal resolution is $dx = 0.2$ m, while the vertical resolution exponential increases in case of the nonuniform grid. Since the grid parameterization of $\beta = 2/3$, $\alpha = 0.1$ and $dz_{max} = 0.8$ was identified as reasonable choice in Section 4.3.2 for the homogeneous halfspace model, it is applied for the heterogeneous models as well.

4.3.4 Resampling of Material Parameter

In case of an heterogeneous model the question of resampling of material parameter arises, because the material parameters are no longer defined at the same locations. Therefore, the following approach is chosen: The true model parameter are assumed to be defined on the uniform grid. Then for each of the grid points of the regular grid, the closest grid point on the nonuniform grid is detected and all points, that share this closest neighbor are pooled in sets. Now, the value of each parameter on the nonuniform grid is calculated by the arithmetic average all points of the corresponding set. If the set is empty, meaning that non of the uniformly spaced grid points has that point as the nearest neighbor, linear interpolation is used.

This procedure can be formulated as matrix vector operation by introducing a sampling matrix $S \in R^{\hat{N}_z \times N_z}$, the original model $m \in R^{N_z \times N_x}$ and the averaged model $\hat{m} \in R^{\hat{N}_z \times \hat{N}_x}$:

Table 4.9: Material Parameter for the Model 2: One Layer Overlaying Homogeneous Halfspace

	depth	S wave velocity v_s	P wave velocity v_p	density ρ
1. layer	0 m	300 m/s	500 m/s	1800 kg/m^3
2. layer	5 m	700 m/s	1200 m/s	2000 kg/m^3

$$Sm_j = \hat{m}_j \tag{4.3}$$

where $\hat{m}_j$ and m_j denote the j-th column of the model matrix. Since the discretization is uniform in the horizontal direction, an averaging scheme is only necessary in the vertical direction.

4.3.5 Model 2: One Layer Overlaying Halfspace

As the first step, a simple heterogeneous model is examined. For this purpose, one layer with lower velocity is added above the homogeneous halfspace. The material parameter of both layers can be found in Table 4.9. In Figure 4.4 the relative error is plotted as a function of offset. The uniform grid performs well and exhibits an error below 0.5%, wheras the solution of the nonuniform grid has an error of approximately 3 % for all offsets. A possible explanation for this relatively high derivation is the positioning of the interface between the first and second layer. In contrast to the uniform grid, the nonuniform is not aligned with the material discontinuities and therefore can not describe the model precisely at that crucial location. To illustrate the effect on the waveform, the computed seismogram of the receiver with greatest offset is presented in Figure 4.5.

4.3.5.1 Variation of Interface Depth

To investigate the effect of the deviation of the grid points and the model discontinuities, Model 2 is slightly perturbed by variation of interface depth between 2.2 m and 4.0 m in steps of 0.1 m. Due to limited computational resources the model space is chosen smaller (length 40 m, depth 20 m, simulation time 0.35 s) and only the first 14 receivers are used. Solutions are computed by using a uniform grid ($dx = 0.2$ m), the proposed nonuniform grid with and without resampling of material parameter and the proposed uniform grid with additional structural grid points. This local refinement of the grid aims at showing, that the problem of alignment of the grid and the model discontinuities can be solved by adopting the grid, such that high contrast regions can be accurately modelled. This is done by arranging the grid in a way, such that the interface is positioned centrally between two grid points while preserving the distance of grid points in that part of the model. Thereby, the discontinuity is represented by a strong gradient centered at the interface location.

In Figure 4.6 the mean relative error depending on the interface depth is shown. In case of the uniform grid, an alternating behaviour of curve can be observed. This is due to the fact, that the grid spacing is twice as big as the step size of variation of depth,

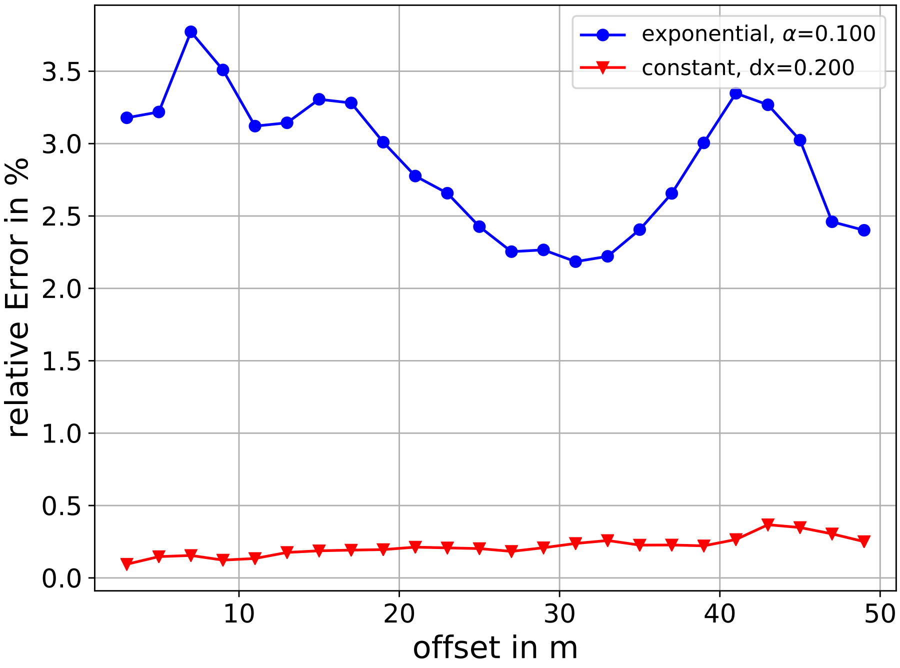

Figure 4.4: Relative error in dependency of receiver offset of Model 2: One Layer Overlaying Homogeneous Halfspace

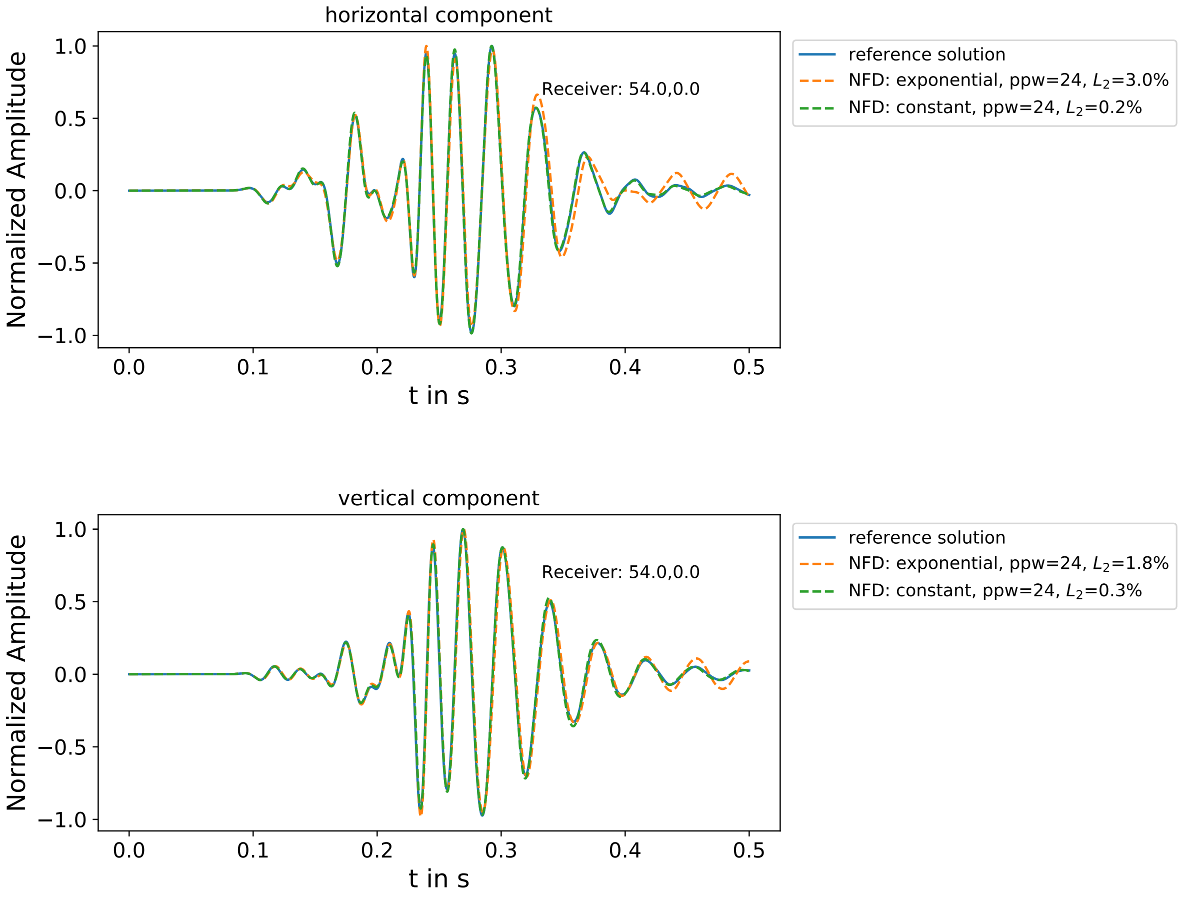

Figure 4.5: The vertical and horizontal velocity component of the receiver with maximum offset of Model 2: One Layer Overlaying Homogeneous Halfspace

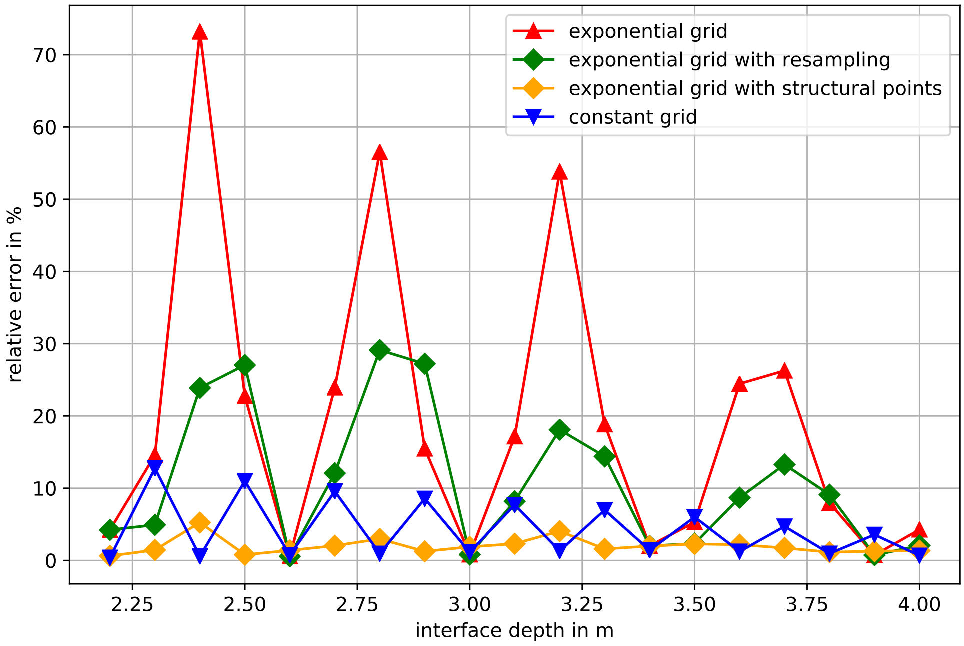

Figure 4.6: Relative error in dependency of the interface depth

resulting in a better representation of the interface every second interface depth tested. Regarding the nonuniform grid without resampling of parameter, the effect of different depths of the interface is large and also shows oscillating behavior. This supports the thesis, that the major part of the error is caused by the location of the interface due to the positioning of grid points, which variantly represents the true location or deviates from it. The resampling and averaging of material parameters leads to a decrease of maximum error, but still does not reach a good level of accuracy. The idea of rearranging the grid at the critical location provides good accuracy (below 5 % of error) independent of the interface depth. The mean relative error over all interface depths is even lower than the error of the uniform grid solution. Apart from that, the error decreases with greater depth of the interface for all grid types. This is caused by the lower sensitivity of the Rayleigh wave to the deeper part of the model.

4.3.6 Model 3: Gradient Increase Overlaying Homogeneous Halfspace

As a second heterogeneous model, a linear gradient increase of all material parameters above a homogeneous halfspace is chosen. The material parameter are defined in Table 4.10. Again, the relative error at different receiver locations is considered (Figure 4.7). Both the uniform and the nonuniform grid perform roughly equally well in this case. The error rises slightly with offset, but only reaches a level of approximately 0.5 %, which can be considered very small. This good result of both methods is likely to be caused by the absence of challenging strong contrast in this model.

Table 4.10: Material Parameter for the Model 3: Gradient Increase Overlaying Homogeneous Halfspace

	depth	S wave velocity v_s	P wave velocity v_p	density ρ
1. layer	0 m	300 m/s	500 m/s	1800 kg/m^3
gradient increase	0 m to 5 m	linear	linear	linear
2. layer	5 m	700 m/s	1200 m/s	2000 kg/m^3

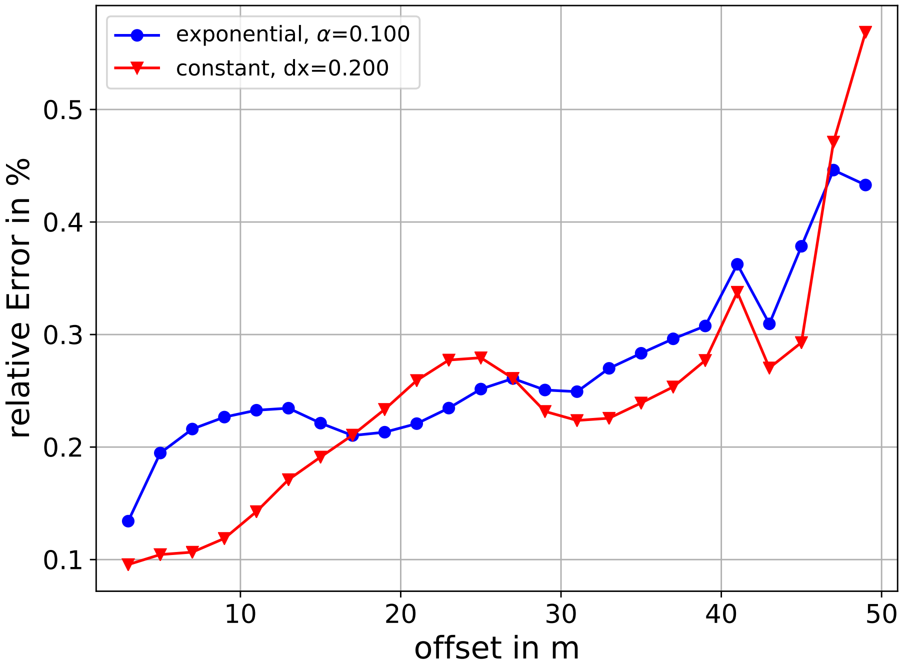

Figure 4.7: Relative error in dependency of receiver offset of Model 3: Gradient Increase Overlaying Homogeneous Halfspace

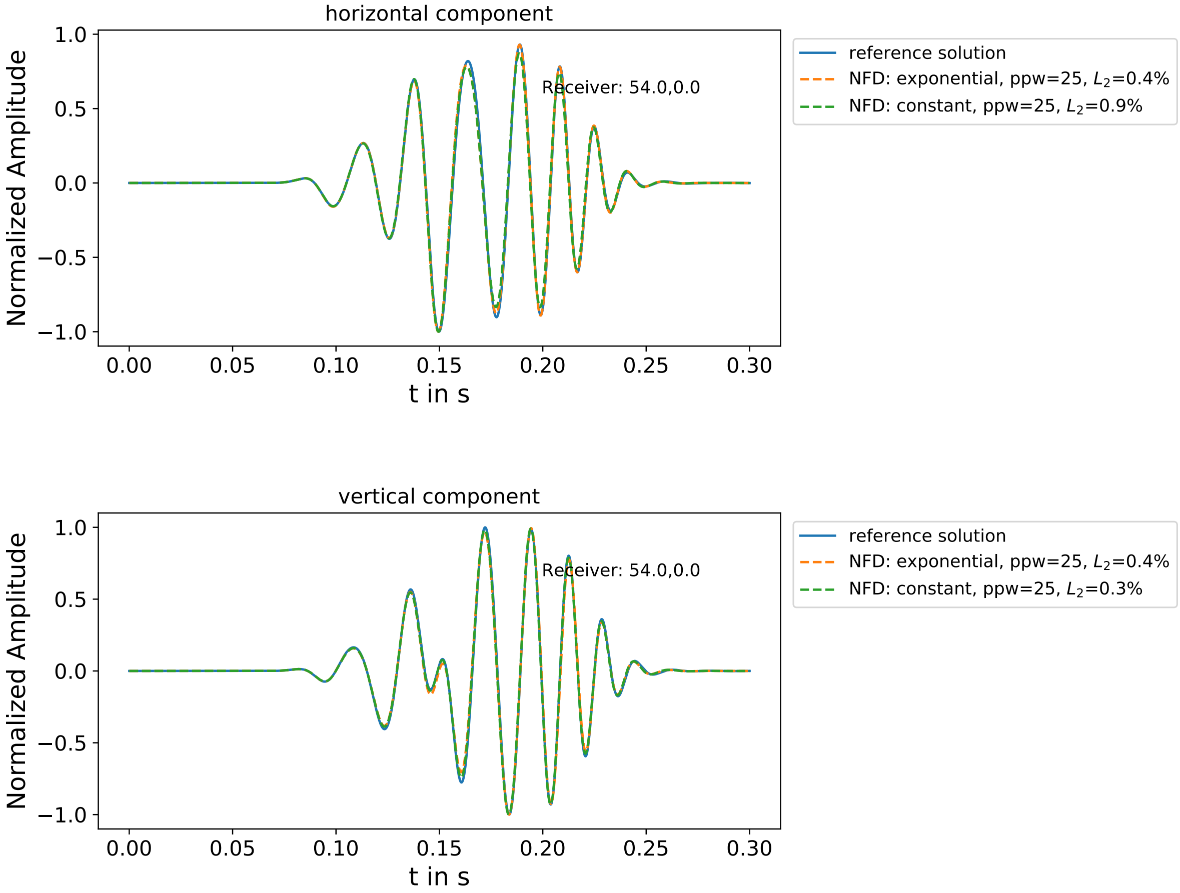

Figure 4.8: The vertical and horizontal velocity component of the receiver with maximum offset of Model 3: Gradient Increase Overlaying Homogeneous Halfspace

4.3.7 Model 4: Low Velocity Layer

Next, a more challenging and complex model is considered. It consist of two layers above a homogeneous halfspace, with the second layer featuring lower velocities than the layer above. This again rises the problem of correct locations of the internal discontinuities. Additionally, the loss of resolution with depth might become relevant because of the low velocity zone in the deeper part. The relative error shown in Figure 4.9 reveals, that the error of the nonuniform grid almost reaches 5 % at the greatest offset. The uniform grid also faces a loss of accuracy, which is not as severe, but still attains a value of 3 % at the maximum. Again, the computed seismogram of the last receiver can be found in Figure 4.10. Taking the complex waveform recorded at this receiver into consideration, both the uniform and nonuniform solutions can be considered relatively accurate.

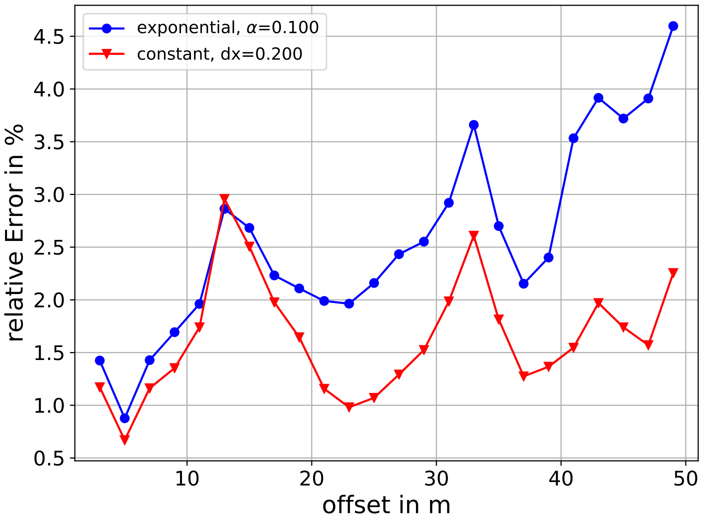

Figure 4.9: Relative error in dependency of receiver offset of Model 4: Low Velocity Layer

Table 4.11: Material Parameter of Model 4: Low Velocity Layer

	depth	S wave velocity v_s	P wave velocity v_p	density ρ
1. layer	0 m	300 m/s	700 m/s	1800 kg/m^3
2. layer	5 m	200 m/s	500 m/s	1700 kg/m^3
3. layer	8 m	700 m/s	1200 m/s	2000 kg/m^3

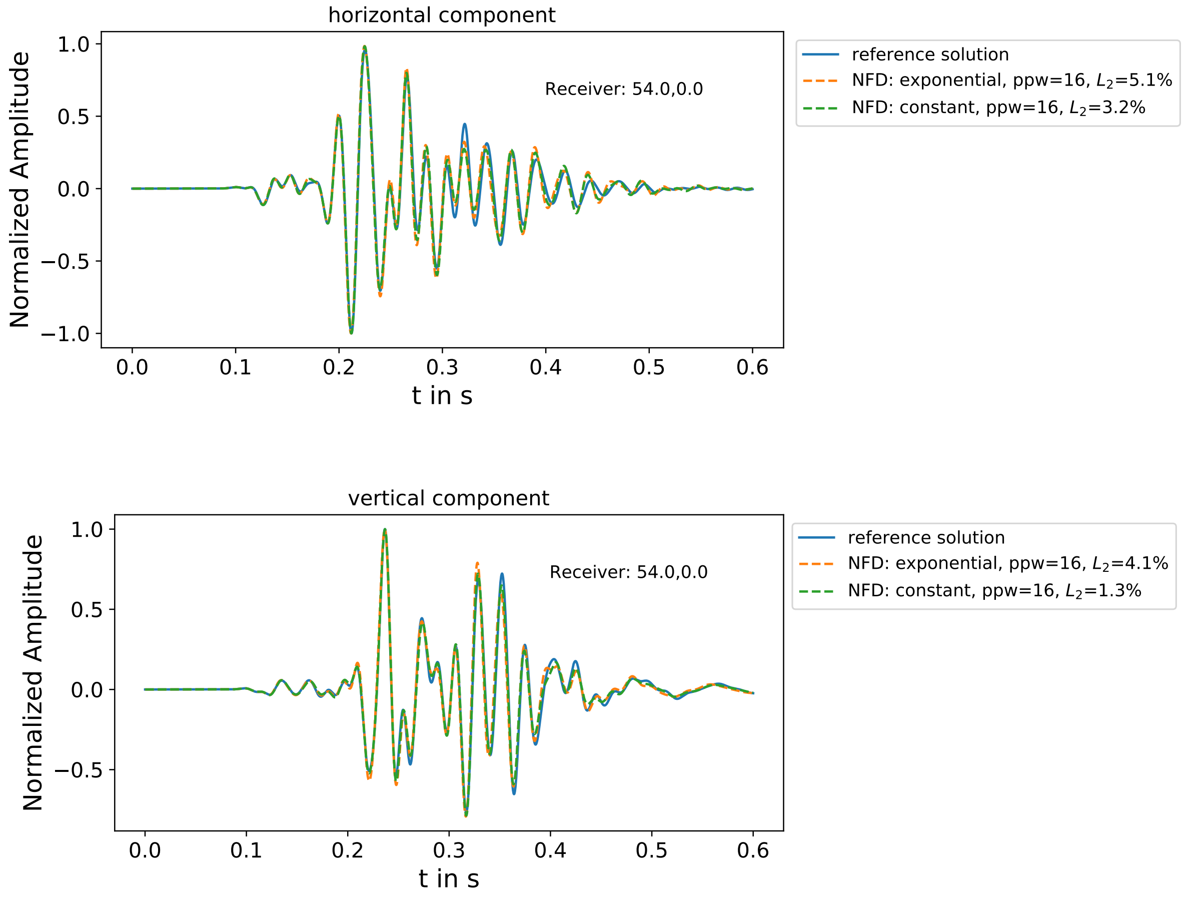

Figure 4.10: The vertical and horizontal velocity component of the receiver with maximum offset of Model 4: Low Velocity Layer

4.3.8 Model 5: Topography Overlaying Homogeneous Halfspace

In this section a model with surface topography is investigated. This is case of special interest, since it currently can only be modelled accurately at high computational expense. This is due to the high spatial resolution, that is necessary to avoid numerical artifacts of the staircases of the discrete surface modelling. Bohlen and Saenger (2006) report, that even up to 60 grid points are not sufficient to achieve accurate solutions, which prohibits the application in case of large 3D models. Therefore, the nonuniform grid approach is of particular interest in this case, as it provides a possibility to achieve the necessary resolution in the upper part of the model, while keeping the resolution in the deeper part and thereby the computational effort low.

The model is constructed as a rising plane free surface with a slope of 20 % above a homogeneous halfspace. Receiver placement is adopted to this configuration and all receivers are located at the surface. The grid spacing is kept constant above depth 0 m, which corresponds to the deepest point of the free surface. The material parameter can be found in Table 4.12. To further illustrate this, a snapshot of the wavefield can be found in Figure 4.12.

In Figure 4.11 the relative error in dependency of the offset from the source is shown. This reveals, that the nonuniform grids delivers a more accurate solution, especially for far offset traces. This is likely to be caused by the finer grid spacing in the vertical direction of the nonuniform grid compared to the uniform grid. As a conclusion, the expected benefit of the nonuniform grid spacing actually eventuates in the considered case.

Table 4.12: Material Parameter of Model 5: Topography Overlaying Homogeneous Halfspace

	depth	S wave velocity v_s	P wave velocity v_p	density ρ
1. layer	0 m	200 m/s	450 m/s	1800 kg/m^3

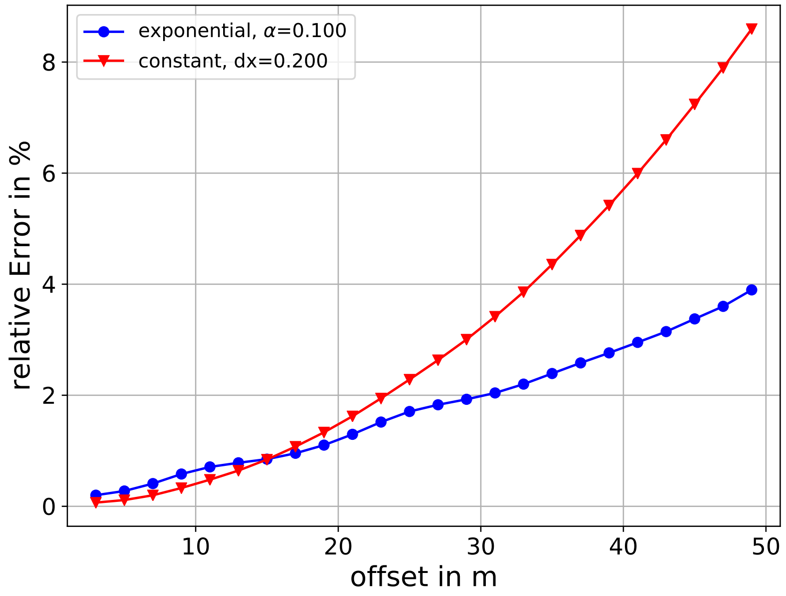

Figure 4.11: Relative error in dependency of receiver offset of Model 5: Topography Overlaying Homogeneous Halfspace

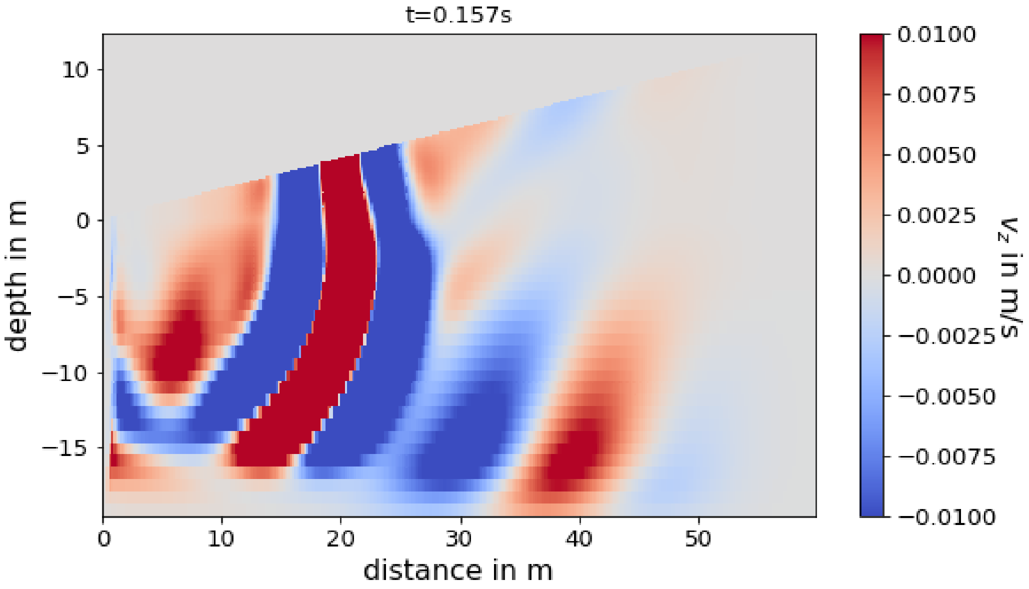

Figure 4.12: Snapshot of the wavefield (v_z-component) of the nonuniform grid of Model 5: Topography Overlaying Homogeneous Halfspace

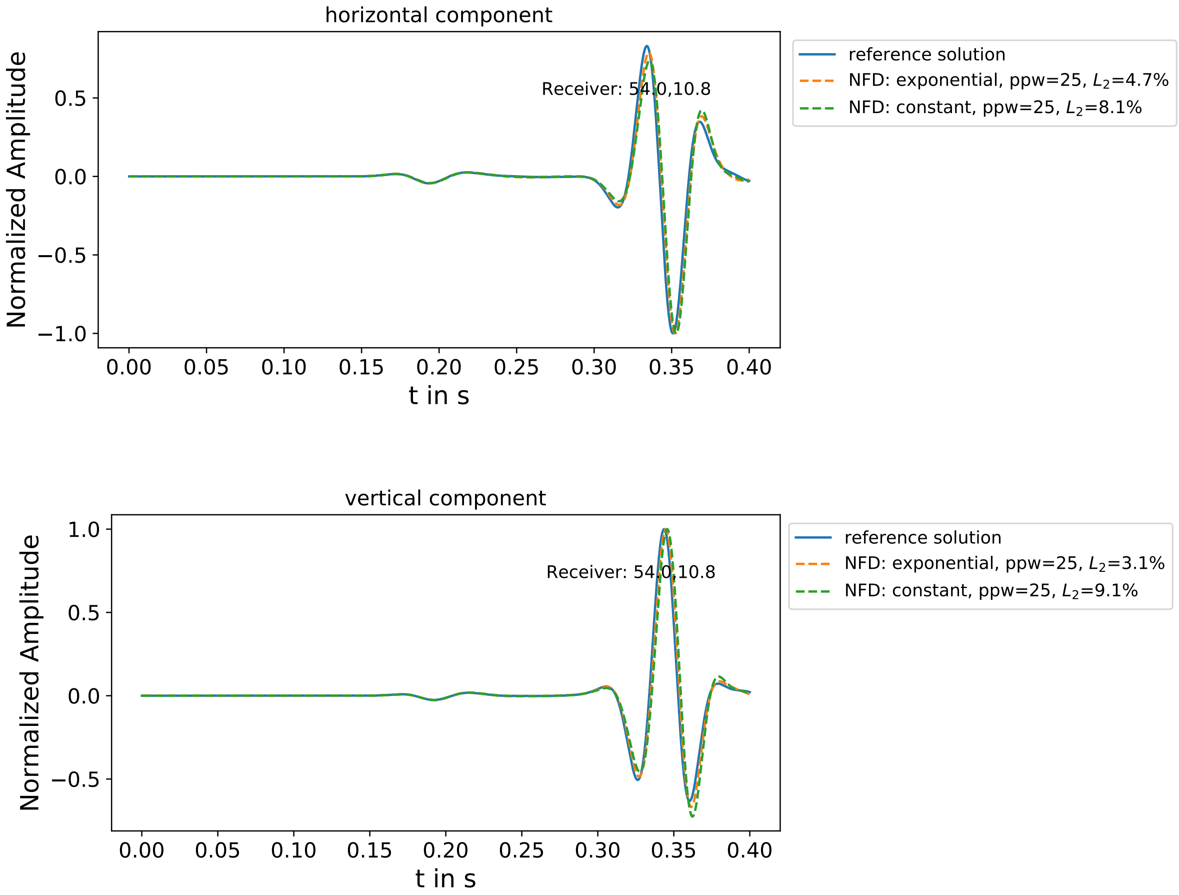

Figure 4.13: The vertical and horizontal velocity component of the receiver with maximumoffset of Model 5: Topography Overlaying Homogeneous Halfspace

4.3.9 Model 6: Vertical Fault with Low- and High-Velocity Bodies

To further test the proposed nonuniform discretization ($\beta = 2/3$, $\alpha = 0.1$), a laterally heterogeneous vertical fault model with a low- and high-velocity body is examined (Figure 4.14). The model size and the placement of receivers are the same as for the homogeneous model. The source is modelled using a Ricker wavelet with a main frequency of 50 Hz. The comparison of the calculated seismograms presented in Figure 4.15a reveals that the proposed nonuniform grid approach provides a high accuracy, even for the complex model considered. The mean relative error of the horizontal and vertical component is $\approx 0.9\,\%$. The accuracy in the waveforms simulated by using the non-uniform grid is equivalent to the result of a uniform grid with $dx = dz = 0.2\,\mathrm{m}$, leading to a saving of 45 % of computational resources while preserving the same level of accuracy.

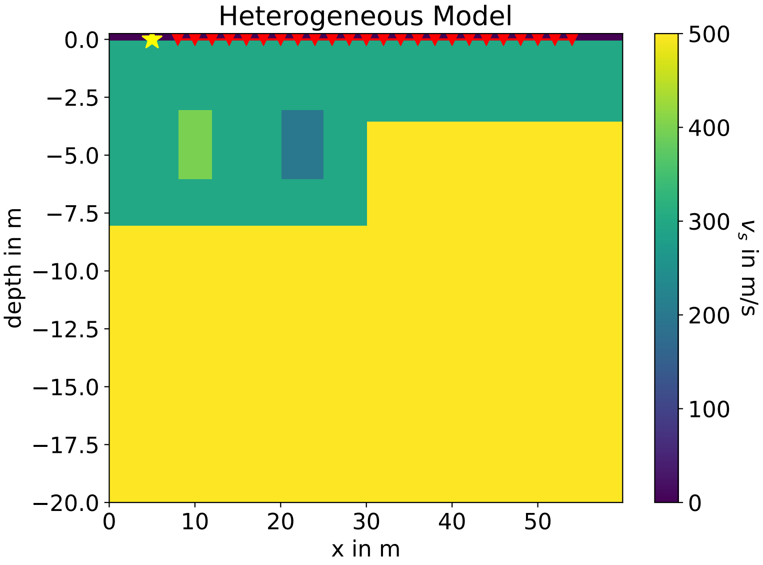

Figure 4.14: Heterogeneous benchmark model with a vertical fault, a low and fast velocity anomaly. The density is set constant across the whole model and the v_p/v_s ratio is 2.25 (except from the air). The yellow star indicates the location of the source and the red triangles represent the receivers.

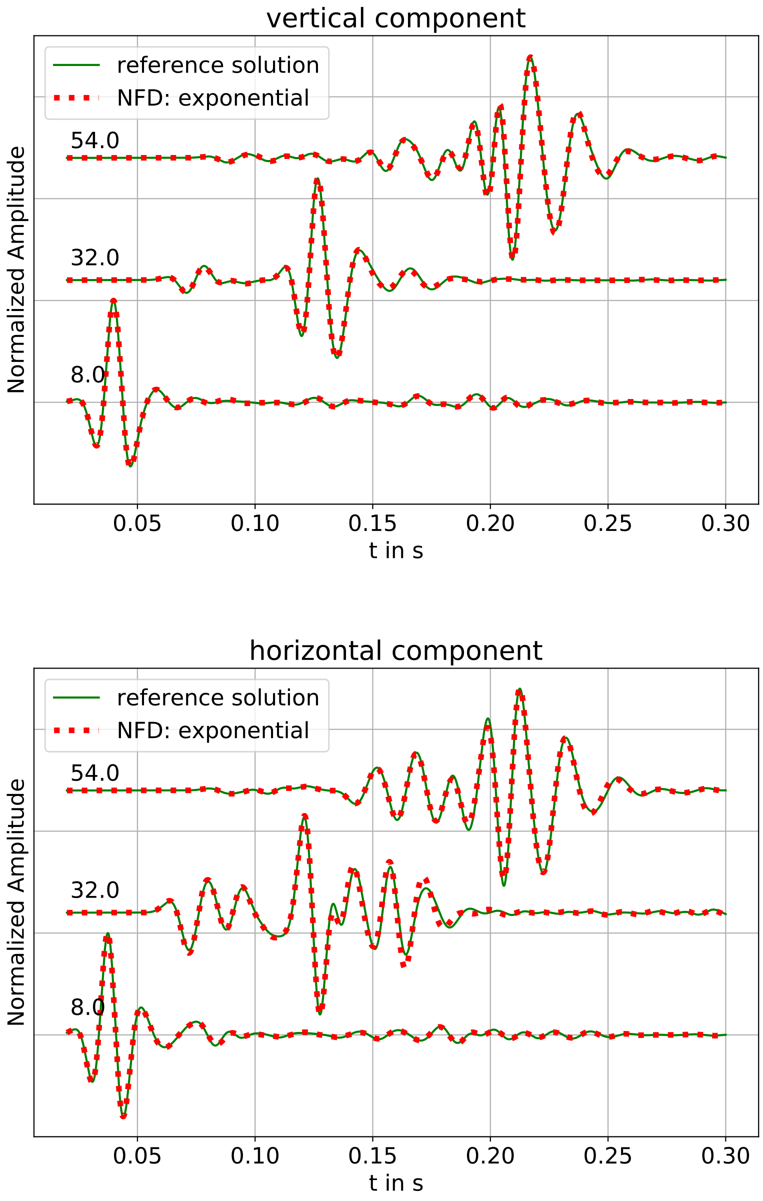

Figure 4.15: Comparison between the synthetic waveforms of the vertical fault model acquired at 8, 32, and 54 m, which corresponds to the first, middle and last receiver.

5 Conclusion

In this chapter a summary of the results obtained in the thesis regarding the research questions formulated in Section 1.3 is given. Additionally, an outlook on further research topics and questions arising from the achieved results is presented.

5.1 Summary

In this work an approach to finite difference modelling of seismic waves in the presence of a free surface on a nonuniform grid has been discussed. It aims at improving the trade-off between accuracy of the simulated solutions and the computational cost by providing the possibility to adopt the grid resolution to the requirements of the model of the subsurface.

The first research question asked for the general ability of the finite difference on grids with nonuniform spacing to deliver reasonable and accurate results. In Section 4.2 and Section 4.3.2 this questions has been answered by first showing the convergence of the implemented algorithm towards the analytical solution for the homogeneous halfspace with decreasing but uniform grid spacing. To classify the accuracy achieved in this numerical test, it has been compared with the results of SOFI2D, a well established finite difference software developed at the Chair of Applied Geophysics at KIT. As a next step, the results of various nonuniform discretizations of the model have been compared to the analytical solution, revealing that the nonuniform finite difference method actually delivers high accuracy solutions of the seismic wave problem in presence of a free surface.

Section 4.3.2 also gives answer to the second research question, that aims at the relation of computational cost and accuracy of the modelling with nonuniform grid spacing. Therefore, an exponential increase of grid spacing with depth has been proposed, taking the spacial characteristics of the Rayleigh wave into account. This discretization model has been parameterized and evaluated by examination of the resulting computational cost, measured by the product of the number of grid points and necessary time steps, and the accuracy obtained. As a result, it can be reported that the saving of computational time and memory and improvement of the level of accuracy can be achieved simultaneously in case a homogeneous halfspace. The effect of nonuniform grid spacing when modelling heterogeneous models of the subsurface has been investigated in Section 4.3.3. It has been shown that the accuracy of the nonuniform grid highly depends on the structure of the model. This is suspected to be caused by the need to average material parameter and the problem of locating material discontinuities at the correct position, if the position is not aligned with the grid. Subsequently, the error of the simulation can be traced back to two different causes: the error of the finite difference method due to the truncation of the Taylor series expansion of the differential operators and the error resulting from the unprecise representation of the original model. To avoid the latter, simple refinement strategies of the computational grid have proven to be an effective measure. Finally, the question of the benefit of nonuniform grids in case of heterogeneous media is highly dependent of the model and the chosen grid spacing.

The third research questions asks for a rule of thumb for the nonuniform discretization. Based on the results of Section 4.3.2, an exponential increase of grid spacing with depth, where each grid distance is enlarged by 10 % in relation to the previous, and a ratio of minimal vertical grid spacing and horizontal grid spacing of 2/3 is proposed in case of the homogeneous halfspace. It provides a saving of 45 % of computational effort compared to a uniform reference grid , while significantly increasing the accuracy. Generally, the realized computational saving rises with the accuracy demanded. Again, the case of heterogeneous models is substantially more difficult. An optimal nonuniform discretezation can hardly be specified, since this is highly model dependant. It is required to represent the velocity structure of the model and has to be aligned with the internal interfaces of the model.

5.2 Outlook

Although the effect of the nonuniform grid spacing has been soundly investigated in this thesis, still a couple a open questions remain and promising aspects deserve consideration, especially regarding the simulation of heterogeneous models.

First of all, the nonuniform discretization of the subsurface has been limited to an exponential increase with depth in this work. Even if this seems to be a reasonable choice with respect to the characteristics of the simulated waves, other curves of grid spacing with depth might be worth a closer look. Beyond that, more sophisticated approaches to the adoption of the grid to the structure of the model might be necessary to fully exploit the potential of the nonuniform grid spacing. A method to automatically construct a grid, that fits the specific needs of the model taking into account the velocity structure and location of interfaces, is highly desirable. Additionally, the question of an appropriate averaging scheme is crucial to the accuracy of the solutions. A comparison of different approaches to that problem might lead to the identification of an averaging scheme, that increases the benefit of the nonuniform grid.

Moreover, the idea of adopting the grid to the models requirements could be extended to the time discretization, leading to different time stepping in the different parts of the model. This is expected to add additional saving of computational resources, at the price of increasing complexity of the method and its implementation.

Finally, the proposed nonuniform grid spacing is also promising in other fields of application than near surface geophysics. Basically, it can be be highly beneficially in any area, where heterogeneous models cause different resolution requirements in different parts of the computational domain. This might be the case in a wide range of not only geophysical, but also engineering applications.

Bibliography

Berckhemer, H. (1990). *Grundlagen der Geophysik*. Wissenschaftliche Buchgesellschaft.

Berg, P. et al. (1994). “Analytical reference solutions”. In: *Modeling the earth for oil exploration* 77, pp. 421–427.

Bohlen, Thomas, Denise De Nil, et al. (2016). “SOFI2D -seismic modeling with finite differences 2D - elastic and viscoelastic version”. In:

Bohlen, Thomas and Erik H Saenger (2006). “Accuracy of heterogeneous staggered-grid finite-difference modeling of Rayleigh waves”. In: *Geophysics* 71.4, T109–T115.

Collino, Francis and Chrysoula Tsogka (Jan. 2001). “Application of the Perfectly Matched Absorbing Layer Model to the Linear Elastodynamic Problem in Anisotropic Heterogeneous Media”. In: *Geophysics* 66, pp. 294–307.

Fichtner, Andreas (2010). *Full seismic waveform modelling and inversion*. Springer Science & Business Media.

Komatitsch, Dimitri and Roland Martin (2007). “An unsplit convolutional perfectly matched layer improved at grazing incidence for the seismic wave equation”. In: *Geophysics* 72.5, SM155–SM167.

Levander, Alan R (1988). “Fourth-order finite-difference P-SV seismograms”. In: *Geophysics* 53.11, pp. 1425–1436.

Leveugle, Benoît (n.d.). *Finite difference coefficients*. URL: `https://www.sphenisc.com/doku.php/software/algo/finitedifference`.

Lorenzo, Juan M. (June 2014). “Mark E. Everett: Near-Surface Applied Geophysics”. In: *Marine Geophysical Research* 35.2, pp. 175–175. ISSN: 1573-0581. DOI: `10.1007/s11001-014-9218-8`. URL: `https://doi.org/10.1007/s11001-014-9218-8`.

Madariaga, Raul (1976). “Dynamics of an expanding circular fault”. In: *Bulletin of the Seismological Society of America* 66.3, pp. 639–666.

Mittet, Rune (2002). “Free-surface boundary conditions for elastic staggered-grid modeling schemes”. In: *Geophysics* 67.5, pp. 1616–1623.

Pitarka, Arben (Mar. 1999). “3D Elastic Finite-Difference Modeling of Seismic Motion Using Staggered Grids with Nonuniform Spacing”. In: *Bulletin of the Seismological Society of America* 89, pp. 54–68.

Shearer, Peter M. (2009). *Introduction to Seismology*. 2nd ed. Cambridge University Press. DOI: `10.1017/CBO9780511841552`.

Socco, Laura Valentina, Cesare Comina, and Farbod Khosro Anjom (2017). “Time-average velocity estimation through surface-wave analysis: Part 1—S-wave velocity”. In: *Geophysics* 82.3, U49–U59.

Virieux, Jean (1986). “P-SV wave propagation in heterogeneous media: Velocity-stress finite-difference method”. In: *Geophysics* 51.4, pp. 889–901.

Zeng, Chong et al. (2012). “An improved vacuum formulation for 2D finite-difference modeling of Rayleigh waves including surface topography and internal discontinuities”. In: *Geophysics* 77.1, T1–T9.